MASSACHUSETTS INSTITUTE OF TECHNOLOGY

LINCOLN LABORATORY

RAIN-OUTAGE REDUCTION BY DATA STORAGE
IN EHF SATCOM SYSTEMS

R.P. RAFUSE
Group 61

PROJECT REPORT DCA-10

25 NOVEMBER 1980

LEXINGTON   MASSACHUSETTS

ABSTRACT

Site diversity is usually proposed as a means for improving earth/satellite path availability at EHF, because intense rain cells are generally small in diameter. However, there are many applications, such as point-to-point, high-data-rate communications, where site diversity is either very inconvenient or impossible. In such cases, provided the user can accept a short delay, incoming data can be stored and retransmitted at a higher rate once the period of high attenuation has passed. By using statistical long-term attenuation and fade-duration probability distributions gathered at several frequencies and geographic locations, an empirical model for determining the improvement in effective availability created by a given amount of storage time is developed. The model appears to be applicable to all geographical areas where standard climatological data is gathered.

CONTENTS

ILLUSTRATIONS

ILLUSTRATIONS (Cont'd)

ILLUSTRATIONS (Cont'd)

TABLES

I. INTRODUCTION

1.1 Rationale

There are many applications where site diversity is either difficult or impossible for small EHF terminals. The difficulty may be due to factors such as cost, tactics (battlefield communications may preclude the interlinking of terminals by other communications capabilities) or geographic constraints (it may not be possible to acquire real estate the appropriate distance away from a given terminal location). In such cases, it may be useful to store data during periods of high rain-induced path attenuation and transmit at a somewhat higher rate during the next period of low attenuation.

The availability of an earth-satellite path, P_A, is defined as one minus the fraction of the time over an average year that the system path margin is insufficient to maintain the desired link probability of error. In this report only rain is assumed to affect the system path margin; other factors, such as component failure, atmospheric absorption repair time, suntransit, and antenna pointing errors are not considered. If the margin is M (dB), the probability of rain is P_{RAIN}, and the cumulative probability density distribution of attenuation, A, when it is raining, is $P(A>A_o|$given rain), the system availability, for $A_o=M$, becomes

$$P_A = 1 - P(A > A_o) = 1 - P_{RAIN} \cdot P(A > M|\text{given rain}) \quad (1.1.1)$$

There are numerous studies which attempt to link $P(A>A_o)$ with known rain-rate distributions and climatological factors [see, for example, Engelbrecht, 1979; Lin, 1973; Bussey, 1950; Hogg and Chu, 1975; Rogers, 1976; Crane and Blood, 1979; Kaul, Wallace and Kinal, 1980; Ippolito, 1978; and Crane, 1971]. This study does not attempt such linkage, except where absolutely necessary[*], but, instead, looks to see if any "universal" behaviors can be found.

---

[*]or where the author's interest was piqued.

1

In Section 2.1 the basic model elements for the attenuation and fade-duration distributions are presented. A model for the probability of rain is developed in Section 2.2. All of the necessary climatologic data for the locations and time spans for which good attenuation data is available are given in Section 2.3. Section 2.4 contains a rationale for ignoring elevation-angle dependencies and Section 2.5 examines the Fresnel-zone-influenced time structure of rain fading. The measured data for several different sites are detailed in Section 2.6 and the basic inputs to a model for storage-time effects are developed for use in the storage-time model presented in Section 2.7. Finally, an example of the use of the storage-time model is given in Section 2.8.

1.2 Conclusions

The basic conclusions are given in Section III of this report. Essentially, the effective margin M_2 (dB) with storage time of T (minutes), in terms of the margin M_1 (dB) without storage, becomes

$$M_2/M_1 = \left[1 + 0.2 \ T'e^{3.7D_T/D_R}\right]^{0.5} \tag{1.2.1}$$

where D_T is the number of thunderstorm days per year and D_e is the number of days per year of rain (as defined in Section 2.3). This model appears to hold for all climatologic regions of the globe. For a climate similar to that of eastern Massachusetts, where $D_T=19$ and $D_R=117$, a storage time of 10 minutes will provide an effective increase in the path-loss margin of 2.16 times. That is, the system availability at, say, 10 dB is improved to that that would have existed with a margin of 21.6 dB.

2

II. ANALYSIS

2.1 Model Elements - The Lognormal Distribution

If attenuation data is taken over a long period of time, generally in excess of 1 year, the distribution of attenuation during the time it is raining will be found to be lognormal. This lognormal behavior was recognized by Lin [1973] and recently reviewed by Engelbrecht [1979]. In addition, in most cases the distribution of the length of time that the attenuation exceeds a given threshold is also lognormally distributed [Lin, 1973]. Specifically, the attenuation in dB will be distributed as

$$P(A > A_0) = P_{RAIN} \cdot \frac{1}{2} \, \text{erfc} \left[\frac{\ln A_0 - \ln A_m}{\sqrt{2} \, S_A} \right] \qquad (2.1.1)$$

where

$P(A > A_0)$ is the probability that the path attenuation A (dB) exceeds A_0(dB),

P_{RAIN} is the probability that it is raining,

A_m is median value of the path attenuation (dB) during the time it is raining, and

S_A is the standard deviation of lnA during the time it is raining.

For a lognormal distribution the mean is related to the median as

$$\bar{A} = A_m e^{S_A/2} \qquad \text{dB} \qquad (2.1.2)$$

In much the same fashion, the cumulative distribution of fade durations beyond a given threshold, A_0(dB), becomes

$$P(\tau > \tau_0) = \frac{1}{2} \, \text{erfc} \left[\frac{\ln \tau_0 - \ln \tau_m}{\sqrt{2} \, S_\tau} \right] \qquad (2.1.3)$$

where

$P(\tau \geqslant \tau_0)$ is the probability that the fade duration τ (minutes) exceeds τ_0 (minutes),

τ_m is the median fade duration in minutes, and

S_τ is the standard deviation of $\ln\tau$.

The median value of τ is

$$\bar{\tau} = \tau_m e^{S_\tau/2}$$

and it should be realized that τ, τ_m, and S_τ are functions of the chosen attenuation threshold, A_0.

Now, the probability that the rain attenuation exceeds a given threshold A_0 for a time in excess of $\tau_0(A_0)$ becomes the product of 3 terms

$$P_{RAIN} \cdot \frac{1}{2} \text{erfc}\left[\frac{\ln A_0 - \ln A_m}{\sqrt{2}\, S_A}\right] \cdot \frac{1}{2} \text{erfc}\left[\frac{\ln\tau_0(A_0) - \ln\tau_m(A_0)}{\sqrt{2}\, S_\tau(A_0)}\right] \quad (2.1.5)$$

It is hoped that most of the non-time-stationary behavior of rain-induced attenuation can be represented by the first term, P_{RAIN}, and that the next two terms can be considered stationary. If so, a system with no data storage capability and a margin M_1(dB) will have a probability of exceeding M_1 during a rainstorm

$$P(M > M_1) = \frac{1}{2} \text{erfc}\left[\frac{\ln M_1 - \ln A_m}{\sqrt{2}\, S_A}\right] \quad (2.1.6)$$

If a storage time of τ_0 is available then a new, equivalent margin, M_2(dB), can be defined from (2.1.5) and (2.1.6) as

$$\frac{1}{2} \text{erfc}\left[\frac{\ln M_2 - \ln A_m}{\sqrt{2}\, S_A}\right] = \frac{1}{2} \text{erfc}\left[\frac{\ln M_1 - \ln A_m}{\sqrt{2}\, S_A}\right] \cdot \frac{1}{2} \text{erfc}\left[\frac{\ln\tau_0(M_1) - \ln\tau_m(M_1)}{\sqrt{2}\, S_\tau}\right]$$

$$(2.1.7)$$

4

A simple relation is sought for the increase in effective margin, M_2/M_1. The "increase" in margin is really a reflection of the increase in availability gained by storage and discussed by Engelbrecht [1979]. Generally M_2/M_1 will be a function of A_m, S_A, τ_m, S_τ, $\tau_o(M_1)$ and M_1. However, as will be seen, the explicit dependence on all but $\tau_o(M_1)$ is slight.

Because the path-attenuation statistics are complex functions of rainfall-rate statistics and such rainfall statistics are functions of the fraction of the total rainfall contained in thunderstorms (convective rain), it should be expected that M_2/M_1 will have some functional dependence on the probability of occurance of thunderstorms. Such a potential dependence is strengthened by the correspondences found in Section 2.3. In Section 2.7 M_2/M_1 will be found to be a function of the ratio of days/year with thunderstorms to days/year with rain.

2.2 On the Determination of the Probability of Rain

Some of the attenuation data available in the literature is presented as a percent of the year a given attenuation is exceeded and some is presented as percent of the raining time a given attenuation is exceeded. In order to convert from one format to the other, the probability that it will rain must be known. Such a probability of rain also places a lower limit on rain-induced availability; that is, a $P_{RAIN}=0.05$ implies an availability always greater than 0.95.

The value of P_{RAIN} represents an instantaneous measure of the percentage of time it rains. Unfortunately, the available climatological data seldom includes measures of instantaneous rain. The usual statistics given include such measures as yearly totals of precipitation, thunderstorm days, cloudy days, total snowfall and number of days when precipitation exceeded 0.25 mm (0.01 inch).

Correlations between percentage of time a given rain rate is exceeded and the ratio of annual precipitation to number of days with measurable precipitation (0.25 mm) have been observed [see Handbook of Geophysics, 1961]. However, the rain rates are clock-hour rates and not instantaneous

5

values (for example, minute-by-minute or second-by-second) and again the percentages are of a total year not the raining time. Other means must be found to determine P_{RAIN}.

Bussey [1950], in one of the first comprehensive treatments of the effect of rain on EHF path attenuation, determined relationships between instantaneous, 1/2-, 1-, and 2-hour-interval measures of rain rate for Washington, DC. His "instantaneous" measures were 1-minute rates. The longer the interval over which rainfall is determined, the higher the percent of the year it would be effectively raining. That is, if a minute-by-minute determination of rain/no-rain is kept, the percentage of raining minutes out of the total minutes in a year would be a smaller figure than would be yielded by a similar determination of day-by-day rain. The reason for this difference is obvious: most days during which rain falls are not "complete" and many will have only a small fraction of the day with rainfall; however, most rain minutes are not so fractionated[*].

The long-term precipitation data for Washington, DC (taken as the average of National- and Dulles-Airport measurements) is presented in Table 2.2.1. Although the water content of snow varies widely from values probably less than 5% in northern Alaska in January to as great as 20% in the "slushy" spring snowfalls common along the east coast of the US, an arbitrary figure of 10% was chosen to remove snowfall from the total precipitation data (since snow attenuation is much smaller than that produced by rain even at the same "water" rates). Similarly, in order to estimate the number of days of measurable rainfall, the number of days with snow greater than 25.4 mm were subtracted from days of measurable precipitation (perhaps days of snow greater than 2.5 mm would have been more appropriate, but such a measure is not available in the National Summarys of Climatological Data).

If Bussey's [1950] relationships are examined at the very lowest rain rates (and extrapolated somewhat for the 1/2-, 1-, and 2-hour interval values)

---

[*]A more recent analysis of the conversion from one averaging time to another was presented by Lin [1976a].

and if the instantaneous hours/year are set at 500 (for a 1-minute rain rate of 0.13 mm/hour or a total of 2×10^{-3} mm in 1-minute), the ratio, r, of 1/2-, 1-, 2- and 24-hour values to the instantaneous value can be determined. Using the 107-day figure from Table 2.2.1, the 24-hour value becomes 107/365.25 or 0.293. The instantaneous value is 0.057 (500 hours in 8760). The 24-hour value and the intermediate values of r are plotted in Fig. 2.2.1.

The simple power-law relation for r-1 is probably representative of many different climates. As a result, if the fraction of the year given by $D_R/365.25$ is divided by the factor of 5.14 from Fig. 2.2.1, a reasonable value for P_{RAIN} can be obtained. That is, if the number of days of measurable (>0.25 mm) precipitation are reduced by the number of days of snow greater than 25.4 mm and the figure that results is multiplied by the reciprocal of 365.25x5.14, the resulting probability of rain can be written as

$$P_{RAIN} = \frac{D_P - D_S}{(365.25)(5.14)} = 5.3 \times 10^{-4} D_R \qquad (2.2.1)$$

It is expected that such a derived value of P_{RAIN} should be reasonably valid for climates as widely varied as Yuma, AZ, with $D_R=16$ and $P_{RAIN}=0.0085$ to Hilo, HI, with $D_R=282$ and $P_{RAIN}=0.15$.

Lin [1975] has defined P_{RAIN} from 1-hour integration-time data supplied by the Weather Bureau. His values of P_{RAIN} are 1-minute averages set equal to 1/2 of the 1-hour rain rates greater than 0.25 mm/hr. The values he records for different locations compare favorably with those using the D_R approach developed here. In the same paper, Lin [1975] also presents an empirical formula which increases the value of P_{RAIN} obtained from point rain data to account for the increased probability of occurance of rain along a path over that expected at a point. His formula is based on Florida thunderstorm data for terrestrial paths and shows quite substantial increases for moderate length paths (~10 km would increase a point value of $P_{RAIN}=0.060$ to 0.083). For an area like Florida with a high rate of scattered thunderstorms such an increase might well be appropriate. However, because of the natural movement of thunderstorms, the increase should be azimuthly sensitive, Lin's is not;

7

TABLE 2.2.1

LONG-TERM, NOMINAL PRECIPITATION DATA FOR WASHINGTON, D.C.[*]

W_T, Total Precipitation in mm   1004

W_S, Total Snowfall in mm   493

W_R, Total Rainfall in mm
(taken as $W_T - 0.1\ W_S$)   955

D_P, Number of Days Precipitation > 0.25 mm   112.5

D_S, Number of Days Snowfall > 25.4 mm   5.5

D_R, Number of Days of Measurable Rain
(taken as $D_P - D_S$)   107

D_T, Number of Thunderstorm Days   28

[*]Data are averages of National and Dulles Airport measurements.
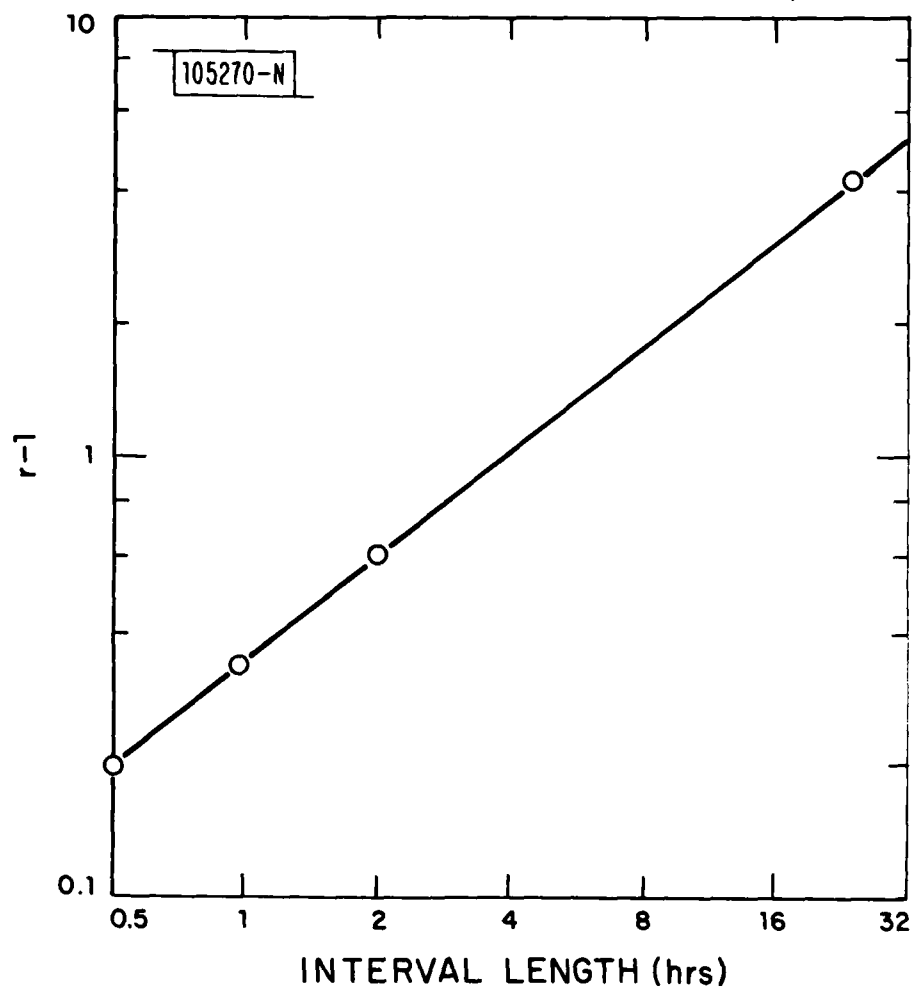
8

Fig. 2.2.1. Values of the ratio of fractional rain time as a function of the measurement interval. Base value is the occurrence of a 1-minute "instantaneous" rain rate of 0.13 mm/hr.

9

moreover, the elevated paths for earth/satellite communications should behave differently than terrestrial paths and other climate areas with a smaller proportion of rain in thunderstorms should show less of an increase. Consequently, such a refinement will not be attempted here and the value of P_{RAIN} for a point, derived from D_R, will be used in the following analyses.

Finally, although the values of P_{RAIN} and relative thunderstorm index, D_T/D_R, where D_T is the number of yearly thunderstorm days, are long-term average values, there can be substantial short-term variability in both measures. If, for some reason, knowledge of the seasonal variability of P_{RAIN} and D_T/D_R is important, a monthly variation can be computed. For a monthly value of P_{RAIN}, called $P_{RAIN,M}$, (2.2.1) can be changed to

$$P_{RAIN,M} = \frac{D_{PM} - D_{SM}}{\text{(days in that month)}(5.14)} \qquad (2.2.2)$$

where D_{PM} is the number of days during that month where precipitation greater than 0.25 mm occurred and D_{SM} is the number of days during that month where snowfall greater than 25.4 mm occurred. If D_{RM} is defined as $D_{PM}-D_{SM}$, then (2.2.2) becomes

$$P_{RAIN,M} = \frac{D_{RM}}{\text{(days in that month)}(5.14)} \qquad (2.2.3)$$

In similar fashion, the monthly thunderstorm-day index, D_{TM}, yields the relative value D_{TM}/D_{RM}.

As an illustration of the potential climatological variations in $P_{RAIN,M}$ and D_{TM}/D_{RM} over the year, average monthly figures for the period 1941 to 1970 were obtained from Ruffner [1978]. The monthly variations for two North-East-Coast-US locations are plotted in Fig. 2.2.2. Two representative Gulf-Coast locations are plotted in Fig. 2.2.3 and two North-West-Coast locations are given in Fig. 2.2.4. A sample of a Central-Plains state and a Rocky-Mountain state is given in Fig. 2.2.5 and two climate extremes for the US, Yuma, AZ and Hilo, HI, are illustrated in Fig. 2.2.6.
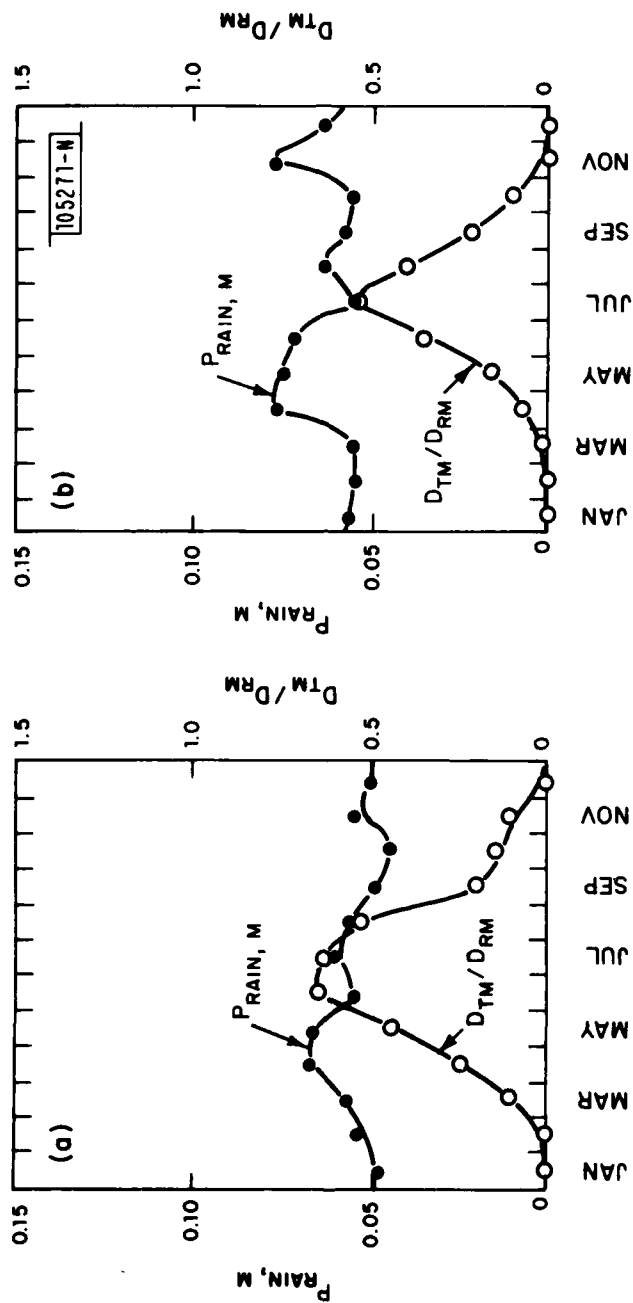
Fig. 2.2.2. Monthly probability of rain and monthly thunderstorm index for two representative North-East-Coast (of the US) locations.

11
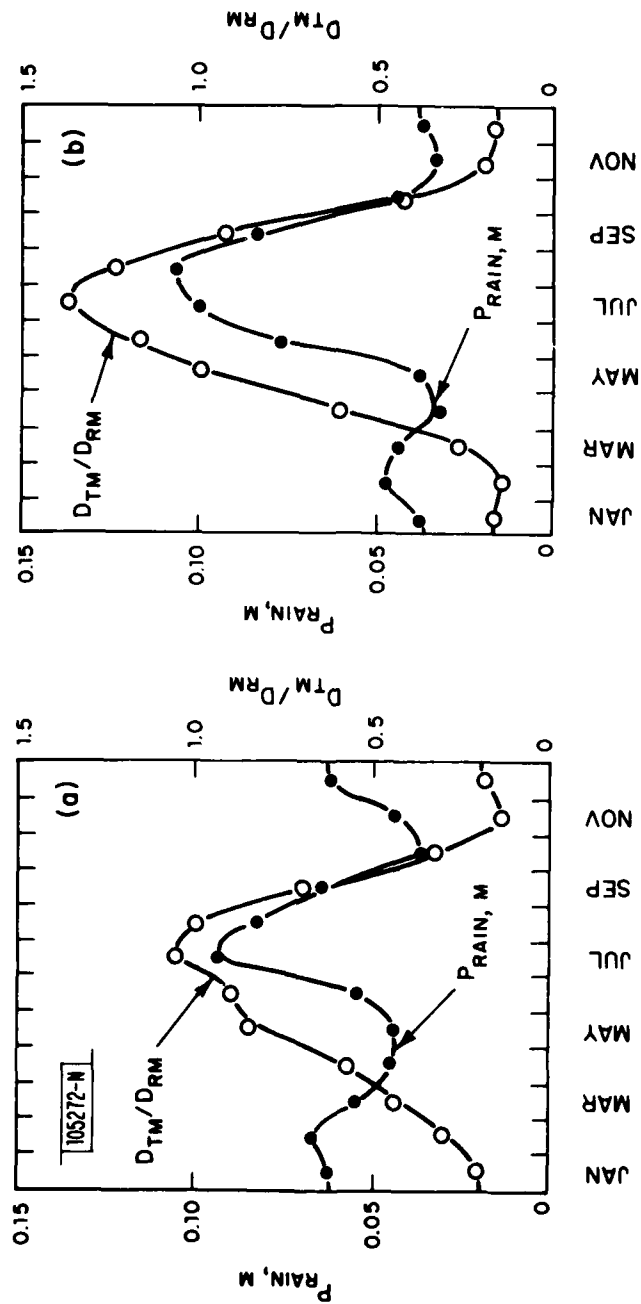
Fig. 2.2.3. Monthly probability of rain and monthly thunderstorm
index for two representative Gulf-Coast locations.

12
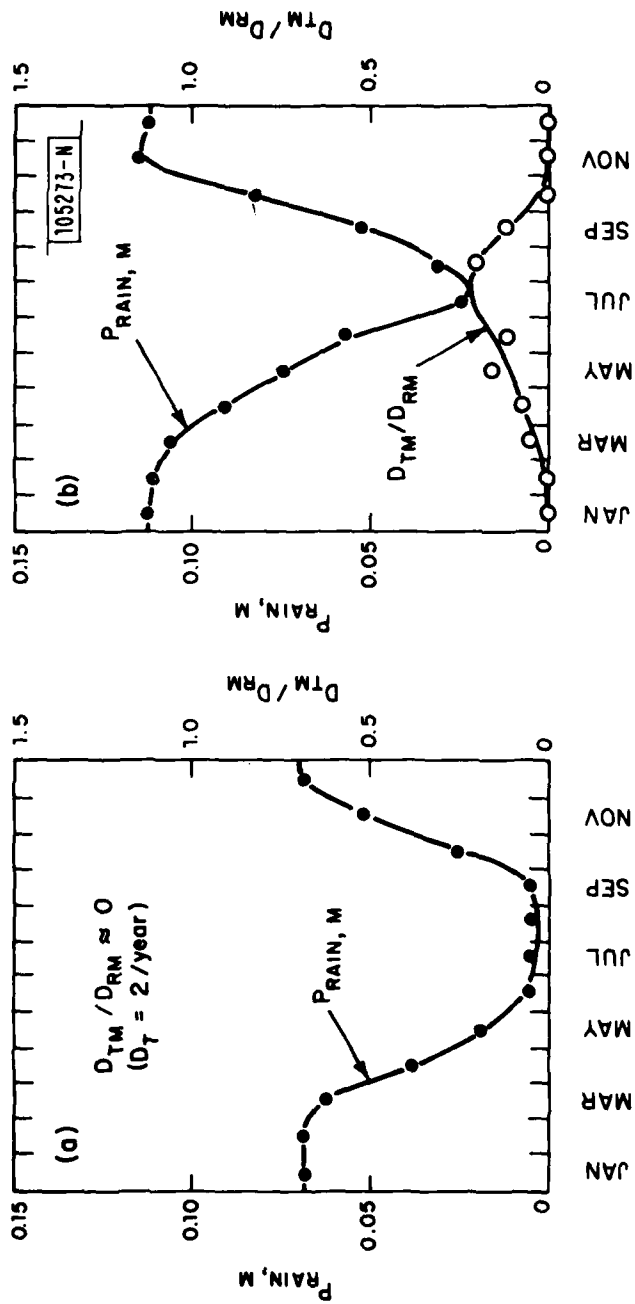
Fig. 2.2.4. Monthly probability of rain and monthly thunderstorm index for two representative North-West-Coast locations.

13

Fig. 2.2.5. Monthly probability of rain and monthly thunderstorm index for a Central-Plains location and a Rocky-Mountain location.
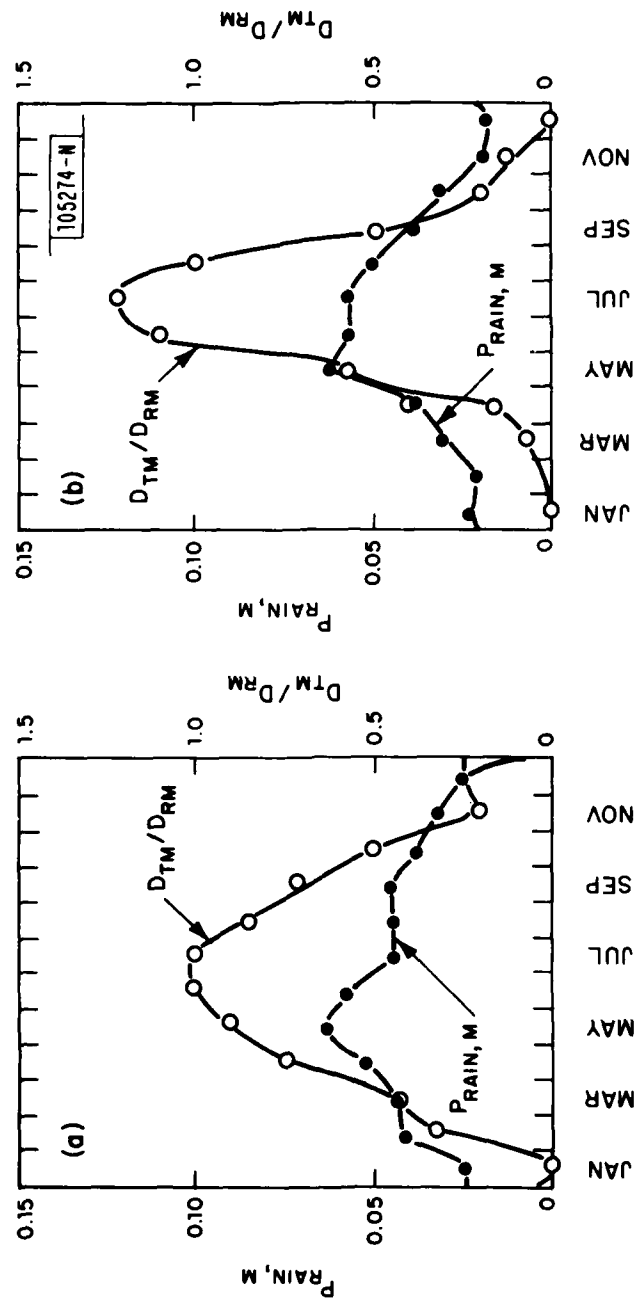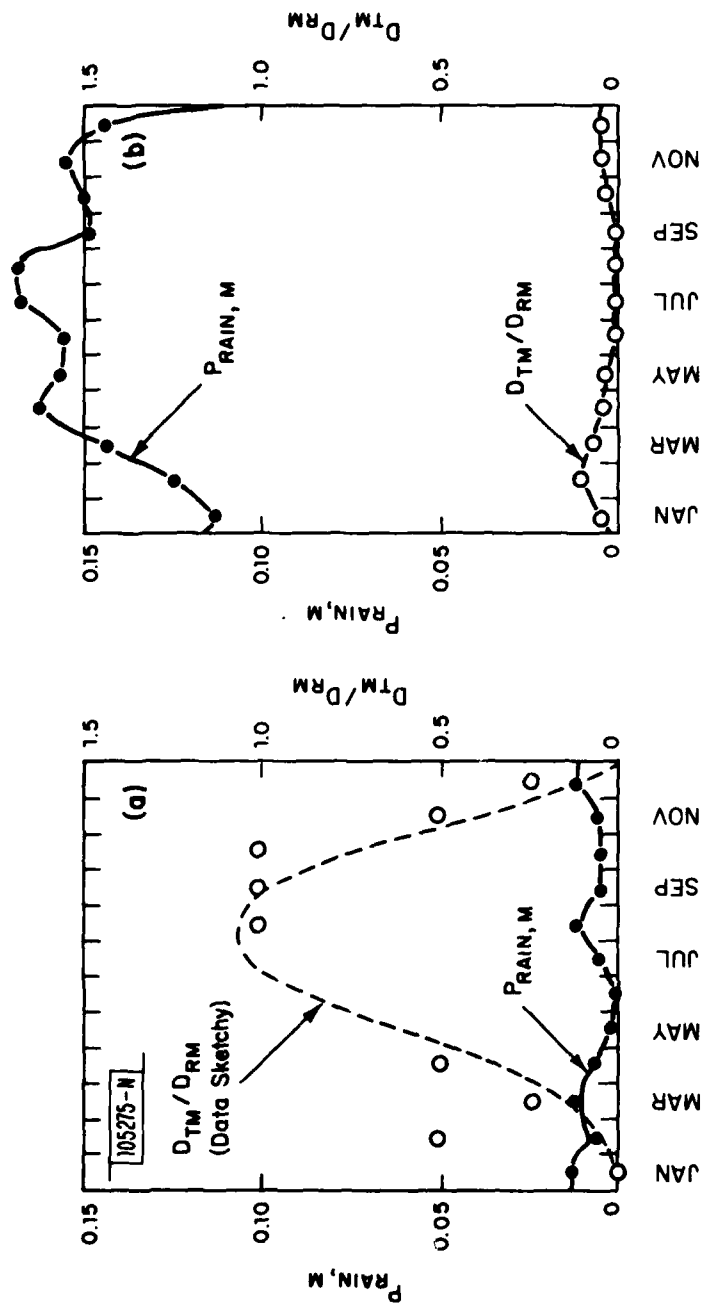
14

Fig. 2.2.6. Monthly probability of rain and monthly thunderstorm index for a desert location, Yuma, AZ, and a very-high rain-probability location, Hilo, HI. These serve to illustrate the climate extremes possible in the US.

15

Several interesting observations can be made. The yearly variability of $P_{RAIN,M}$ on the North-East-Coast and the desert (Yuma, AZ) and Pacific-Island (Hilo, HI) locations is small. "April showers" may "bring May flowers" only in New England. Gulf-Coast locations have a peak in $P_{RAIN,M}$ in the summer months (and a second, minor peak in late winter) with the summer peak the result of much increased thunderstorm activity. On the other hand, the North-West-Coast locations have their "wet seasons" in late fall and winter and the summer months are dry.

The values of P_{RAIN} that result from an average over the year of $P_{RAIN,M}$ for the locations chosen will be slightly different from those used later in Section 2.3. Similar variations in D_T/D_R will be found. The reasons for these differences lie in the different data bases used (1941-1970 versus a much longer-term average). Also, because thunderstorm days are defined as days in which thunder is _heard_, on a monthly basis D_{TM}/D_{RM} can be greater than unity. This behavior will be most pronounced in such locations as New Orleans, LA, Tampa, FL, Denver, CO, and Yuma, AZ, where most of the summer rainfall occurs as thunderstorms and at any given point a thunderstorm may well be heard but no rain falls from that storm on that day at that particular location.

2.3 Climatological Data

The best and most complete long-term data available on rain-induced earth-space path attenuation at EHF comes from sites in Waltham, MA [Nackoney, 1979, and Tang, 1979], Austin, TX [Vogel, 1979], Crawford Hill, NJ [Wilson, 1969 and Lin, 1973], Tampa, FL [Tang, 1979, and Tang, 1980], Slough, ENG [Davis, 1971, and Davis, 1973], and Rosman, NC [Ippolito, 1975 and Crane, 1980]. In order to interpret the data, the climatological data for each area, both nominal and for the period the data were taken, are needed.

The data for the US sites can be obtained from the Climatological Data reports of the National Oceanic and Atmospheric Administration (sometimes called LCD's for Logical Climatological Data). The climatological data for Slough, ENG, were obtained from several sources, including the USAF Environmental Technical Applications Center Worldwide Airfield Climatic Data

[April 1971] and the Handbook of Geophysics [1961], and monthly data were summed to obtain values which cover periods different from one calendar year.

Nominal values for total yearly rainfall, days with rainfall in excess of 0.25 mm, thunderstorm days and probability of rain computed using (2.2.1) are given in Table 2.3.1. The same parameters for the observational periods are given in Table 2.3.2. It is of interest to note that the Crawford Hill, NJ, P_{RAIN} value of 0.056 for 1968, which is obtained from Newark Airport measurements, compares favorably with the value of 0.0523 measured by the experimenters and given by Lin [1972]. In addition, Lin [1972] gives the value of P_{RAIN} for Slough, ENG, as 0.085 which compares favorably with the nominal value of 0.089 and the period value of 0.092 as obtained by this simple modification of daily climatological data.

It is interesting to examine the instantaneous rain-rate curves redrawn taking P_{RAIN} (derived from (2.2.1) and climatological data) into account. Four representative (Middle-East-Coast, Gulf-Coast, Central-Plains, and North-West-Coast) US areas are chosen to exhibit medium, very-high, high and low thunderstorm activities, respectively. Data on rain rates from Washington, DC, New Orleans, LA, Oklahoma City, OK, and Portland, OR, were obtained from the Handbook of Geophysics [1961] as percent-of-year values and changed to cumulative probabilities during periods of rain using P_{RAIN} from (2.2.1) and nominal climatological data. The results are plotted in Fig. 2.3.1.

Note that the low-rate portions of the curves are essentially lognormal and the high-rate portions represent a second distribution largely due to thunderstorm activity[*]. Even Portland, OR, with $D_T=7$, shows some bimodal character. The fall-off at very high rates can be due to lack of sufficient statistics and/or the 1-minute averaging times. Lin (1976b) has proposed a means of estimating the extreme-value statistics. However, if the averaging

---

[*]This difference was also noted by Hogg [1969].

17

TABLE 2.3.1

NOMINAL CLIMATOLOGIC DATA FOR DATA-GATHERING SITES

LOCATION	NOMINAL VALUES			
	W_R, MM[6]	D_R, DAYS[7]	D_T, DAYS	P_{RAIN}[8]
Waltham, MA[1]	971	117	19	0.062
Rosman, NC[2]	1149	119	46	0.063
Austin, TX	823	82	41	0.044
Crawford Hill, NJ[3]	981	115	25	0.061
Tampa, FL	1254	107	88	0.057
Washington, DC[4]	955	107	28	0.057
Slough, ENG[5]	605	167	15	0.089

1. Boston (Logan Airport), MA
2. Average of Greenville, SC and Asheville, NC
3. Newark (Newark Airport), NJ
4. Average of National and Dulles Airport data
5. London (Heathrow Airport), ENG
6. Total precipitation minus one-tenth of total snow, sleet, hail, etc.
7. Number of days precipitation is greater than 0.25 mm minus number of days snow, sleet, is greater than 25.4 mm
8. Taken as 5.07×10^{-4} times D_R

TABLE 2.3.2
PERIOD-RELATED CLIMATOLOGICAL DATA

LOCATION	PERIOD	PERIOD DATA			
		W_R, MM	D_R, DAYS	D_T, DAYS	P_{RAIN}
Waltham, MA[1]	2/77-1/78	1065 (971)	124 (117)	22 (19)	0.066 (0.062)
Waltham, MA[1]	2/78-1/79	855 (971)	103 (117)	11 (19)	0.055 (0.062)
Waltham, MA[1]	2/77-1/79	960 (971)	114 (117)	17 (19)	0.060 (0.062)
Rosman, NC[2]	CY74	1168 (1149)	127 (119)	52 (46)	0.068 (0.063)
Austin, TX	2/78-1/79	819 (823)	89 (82)	17 (41)	0.047 (0.044)
Crawford Hill, NJ[3]	CY68	907 (981)	106 (115)	24 (25)	0.056 (0.061)
Tampa, FL	1/78-12/79	1401 (1254)	107 (107)	82 (88)	0.057 (0.057)
Slough, ENG[4]	6/68-6/72	678 (605)	170 (167)	* (15)	0.092 (0.089)

1. Boston (Logan Airport), MA
2. Average of Greenville, SC, and Asheville, NC
3. Newark (Newark Airport), NJ
4. Taken from Gatwick Airport data and scaled by other known climatological data to Heathrow Airport (e.g., nominal total rainfall at Gatwick is 1.13-times that at Heathrow)
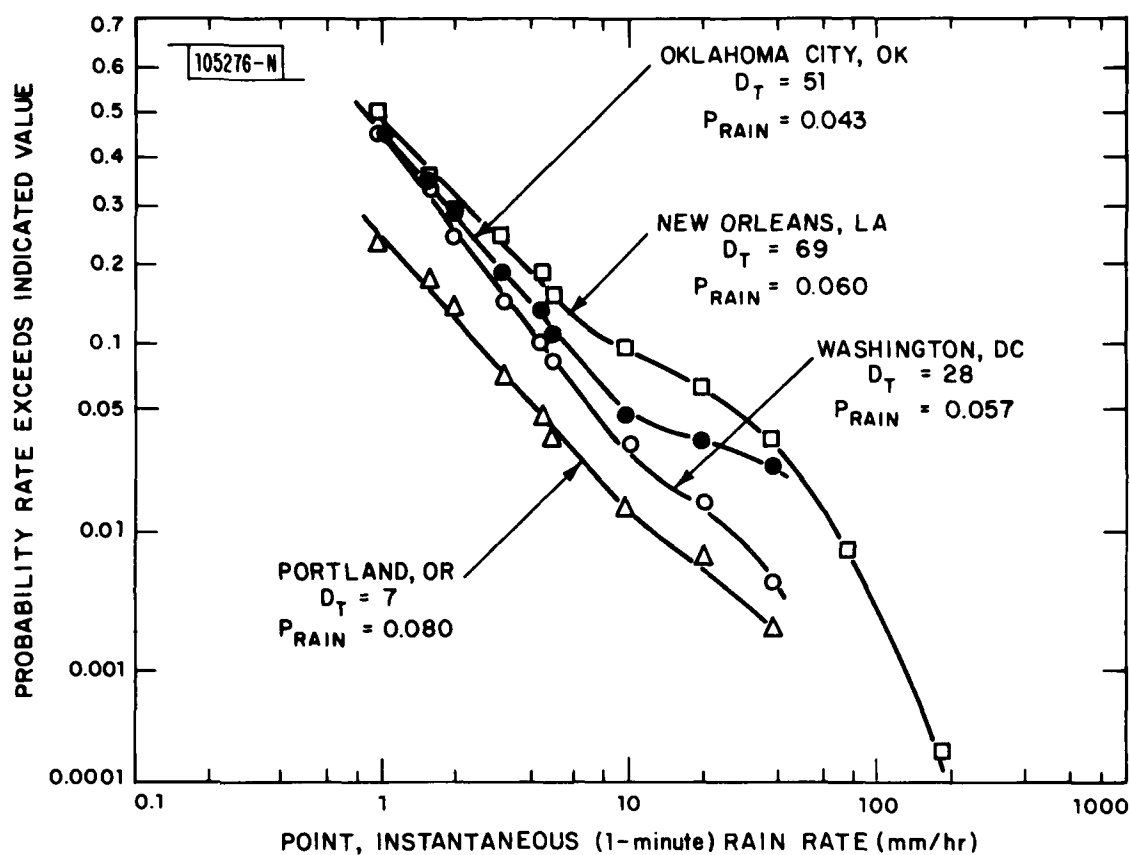
   *Unavailable - Use nominal value

Fig. 2.3.1. Rain-rate distributions for four representative climate areas.

20

times were dropped to 0.1 second or less it is expected that the probability values at the high rates will increase and a second lognormal distribution will be uncovered*.

It is tempting to consider a crude separation into two types of rain, thunderstorm-created and non-thunderstorm-created. If the long-term cumulative statistics for rain-rates, R, are defined as $P_T(R>R_0)$ for thunderstorms and $P_{NT}(R>R_0)$ for non-thunderstorm rain, then a combined cumulative statistic might be written as

$$P(A > A_0) = [D_T/D_R] \, P_T(R > R_0) + [1 - D_T/D_R] \, P_{NT}(R > R_0)$$

$$(2.3.1)$$

where D_T is the number of thunderstorm days and D_R is the number of days of measurable rain as defined in Section 2.2. By using the Portland, OR, and New Orleans, LA, data, two lognormal distributions representing $P_T(R<R_0)$ and $P_{NT}(R>R_0)$ are generated and plotted in Fig. 2.3.2. Their fit to the long-term measured point rain-rate data is illustrated in Fig. 2.3.3.

The agreement in Fig. 2.3.3 provides some further credibility to the empirical P_{RAIN} determination given in Section 2.2 and indicates that the ratio of thunderstorm days to days of measurable rain, D_T/D_R, is likely to be an important parameter in models for EHF satellite-communications systems behavior with rain. It should be noted, however, that the correlation between point rain rate and attenuation is not perfect.

The attenuation from rain is an area phenomena. A relation between maximum rainfall, area over which it is observed, and the duration was obtained by Fletcher [1950]. The relation becomes

$$R_T \approx 12.7\sqrt{T_D} \left[1 + \frac{373}{13.5+D_{km}}\right] \quad \text{mm} \tag{2.3.2}$$

---

*In fact, the maximum point rain rates are bounded by the reciprocal of the square-root of their duration [Fletcher, 1950] and a decrease in averaging time by over two orders-of-magnitude should provide an additional order-of-magnitude in observed long-term rain-rates.
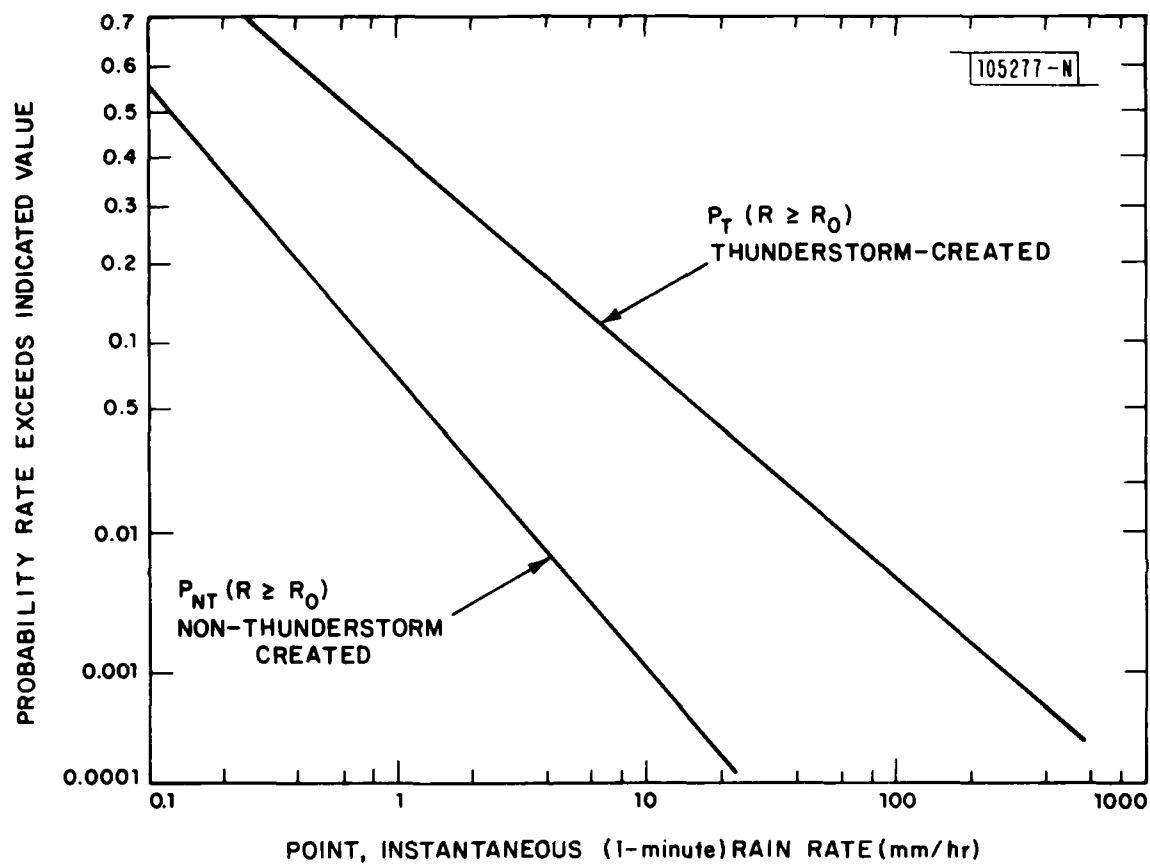
Fig. 2.3.2. Thunderstorm-created and non-thunderstorm-created
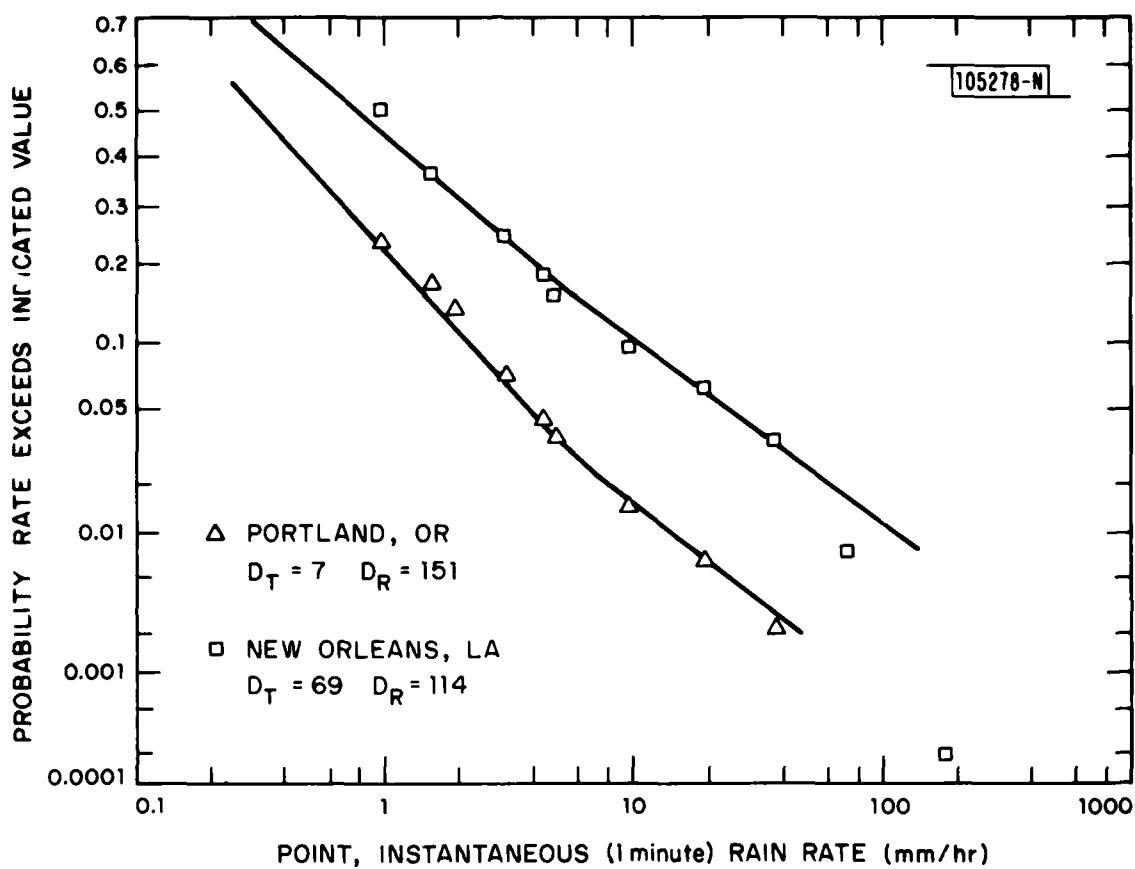rain-rate distributions as derived from Fig. 2.3.1.

Fig. 2.3.3. Reconstructed rain-rate distributions using data from
Fig. 2.3.2. Measured data points are given for comparison.

23

where

R_T is the total rainfall in mm

T_D is the rainfall duration in hours

D_{km} is the diameter in km of the area over which the rain amount, R_t, falls in time T_D

Note that a point rainfall maximum envelope becomes ($D_{km}=0$)

$$R_{T,POINT} = 364\sqrt{T_D} \quad mm \tag{2.3.3}$$

and a wide-area rainfall maximum envelope becomes ($D_{km}=\infty$)

$$R_{T,WIDE} = 12.7\sqrt{T_D} \quad mm \tag{2.3.4}$$

If the "effective" rain rate becomes $R=R_T/T_D$ mm/hr, then it should be expected that the most intense rainfalls should last for the shortest times and extend over the smallest areas. This factor has obvious application in diversity siting as well as "waiting-time" determinations.

2.4 <u>Elevation Angle Dependence</u>

Because the path lengths in the atmosphere are different, it would be expected that two different elevation angles on the same azimuth examined simultaneously during a rainstorm would exhibit different values of attenuation. At low rain rates, where rainfall is generally widespread and relatively homogeneous both in azimuth and elevation (up to the 0°-C isotherm), the isochronal attenuations would be approximately related by the classical $csc\theta$-relationship[*]. However, the more intense rain, particularly that originating in thunderstorms, is by no means homogeneous, either in azimuth or in elevation.

─────────────

[*]Or modifications thereto caused by a spherical earth.

Even simple geometries like the cylindrical rain cell illustrated in Fig. 2.4.1 do not yield simple results. For example, assume the rain extends uniformly to the ground from the melting layer height, h_0 (0°-C isotherm). Even if the edge of the rain cell includes the terminal (R=d/2), the $\csc\theta$ behavior will only be apparent if $d \gg h_0$. If $d < h_0$, as can be the case, for much of the useful elevation-angle range the attenuation due to that rain cell increases with increasing θ. Other more complex geometries will give more complex elevation-angle dependencies.

The yearly behavior of h_0 at two different locations (obtained from National Summaries of Local Climatological Data) is shown in Fig. 2.4.2. Note that melting-layer heights in excess of 4 km are common for those months of the year in which thunderstorms are prevalent. Thunderstorm rain-cell sizes measured by a weather research radar in Goodland, Kansas [Crane, et al., 1977; Crane, 1980] are converted by the relationship for thunderstorm rain rate, R, and radar reflectivity, Z [Rogers, 1976] as

$$Z = 200R^{1.6} \quad . \tag{2.4.1}$$

The data are sparse, but an approximate lognormal[*] behavior is obtained and illustrated in Fig. 2.4.3. Note that as rain rate (and potential attenuation) increases, the median cell diameter drops from about 2.5 km at low rain rates ($\sim$0.5 mm/hr) to about 1.6 km at moderate to high rain rates ($\sim$40 mm/hr). Therefore, most of the time, thunderstorm rain cells will have effective diameters much smaller than their heights and the $\csc-\theta$ behavior for attenuation will not be observed.

In many cases, not only are the rain-cell structures taller than their effective diameters, but they are tilted and distorted by the natural progression velocity of the storm [Goldhirsh, 1976]. Furthermore, there is no guarantee that the rain rates within a given cell will be homogeneous with altitude; such a lack of vertical uniformity is illustrated by Fig. 2.4.4,

---

[*]Similar lognormal size behavior has been observed by Strickland [1974].
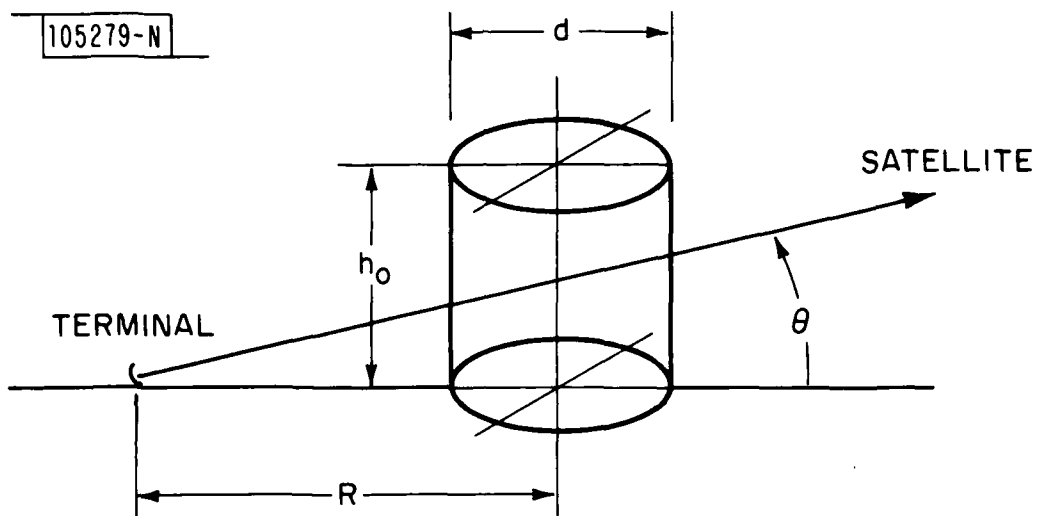
Fig. 2.4.1. Illustration of a simple cylindrical rain-cell geometry with melting-layer height h_0, cell diameter, d, distance from center of cell to terminal of R and satellite elevation angle, θ.
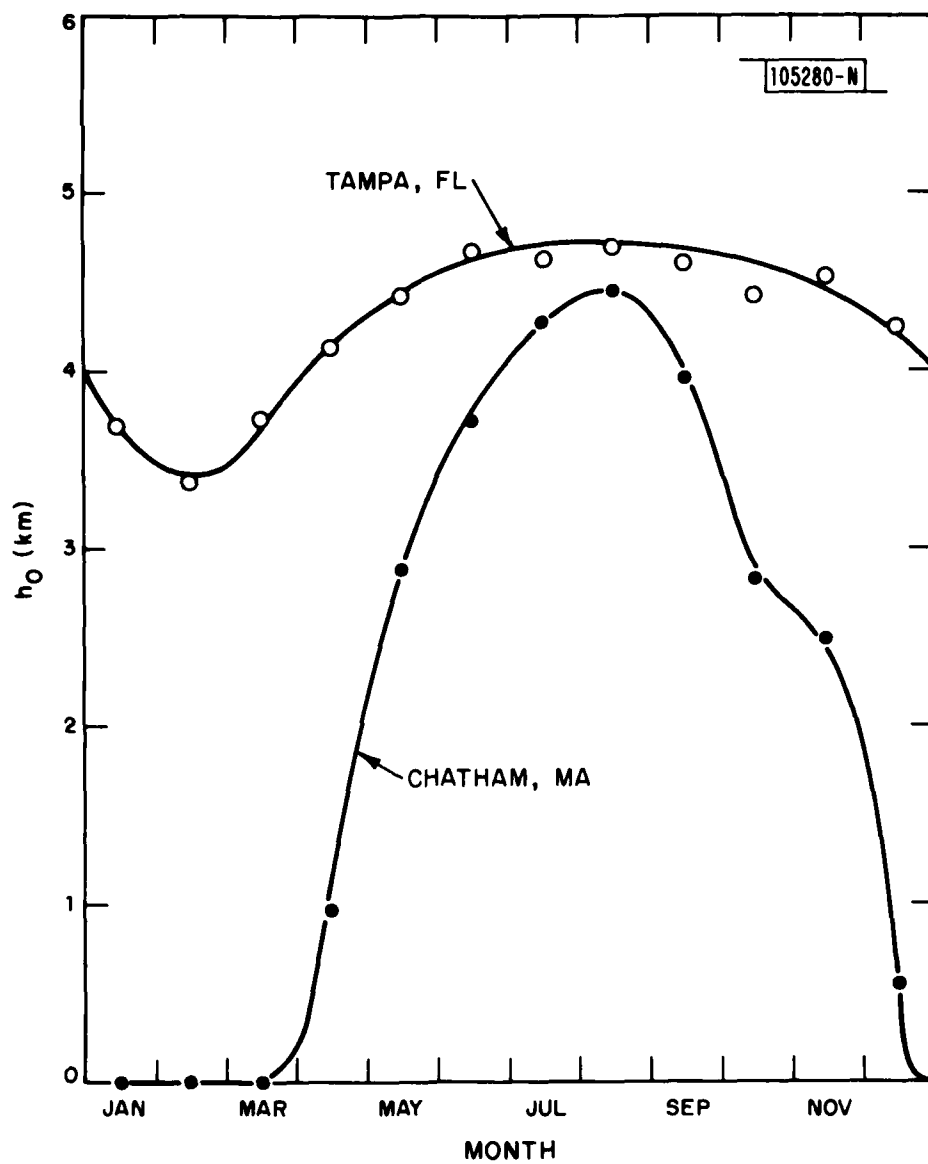
Fig. 2.4.2. Average zero-degree (C) isotherm heights as a function of time over a year for two representative locations.
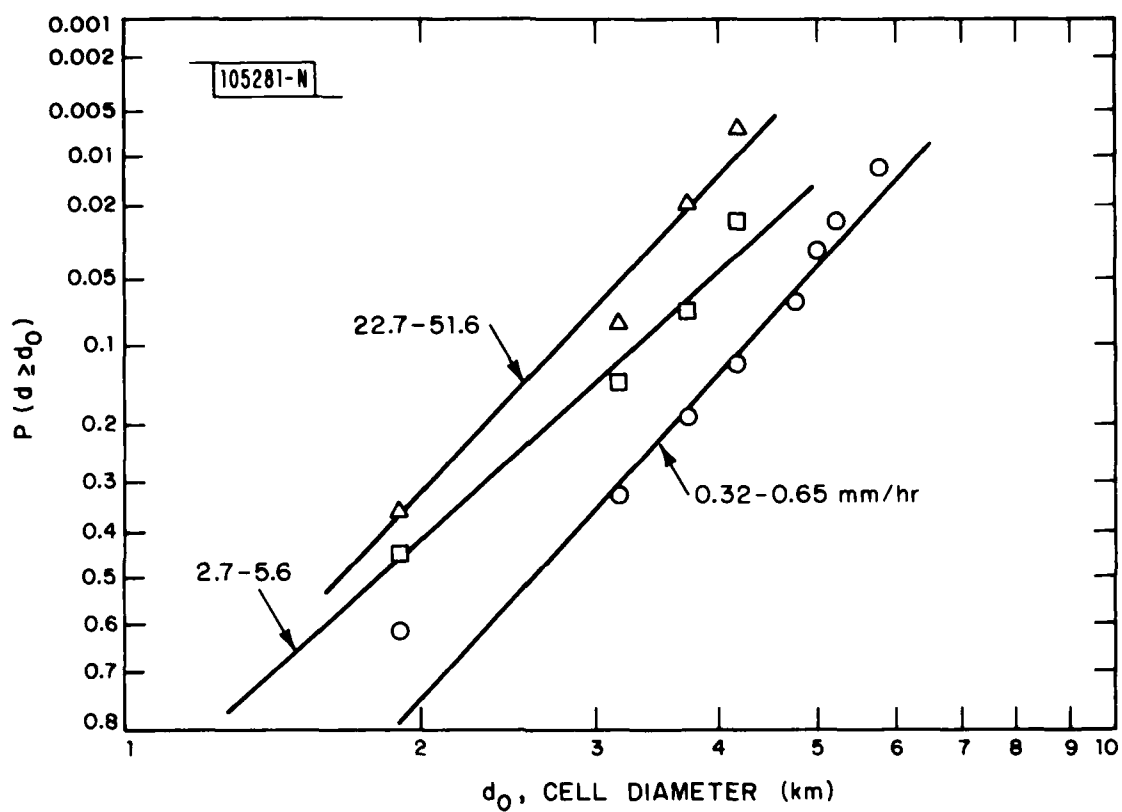
Fig. 2.4.3. Cumulative probability distribution functions for rain-cell diameters with rain rate as a parameter.
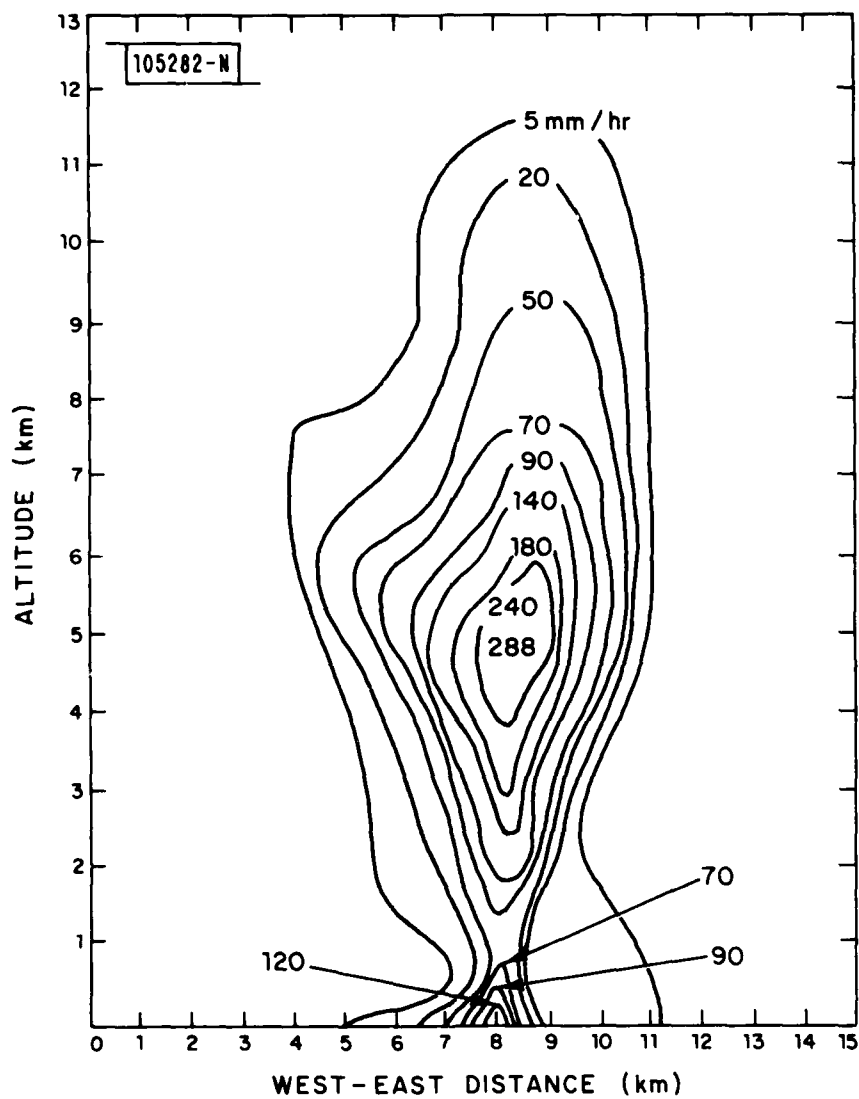
28

Fig. 2.4.4. Radar-derived west-east cut through a thunderstorm.

taken from the Handbook of Geophysics [1961] and based on data obtained by Atlas [1948]. A terminal located at the zero-kilometer reference point and looking east through the storm would experience a peak path rain rate of 288 mm/hour at $\theta=30^\circ$ dropping to 70 mm/hour at $\theta=7^\circ$. It also appears that the cell structure is such that the total path integrated rain rate at $\theta=30^\circ$ would be greater than that observed at $\theta=7^\circ$ by a factor even larger than the ratio of peak path rain rates.

Finally, the atmospheric portion of the earth-space path could well encompass several different rain cells at the same time. A transverse cross-section through a thunderstorm [Crane, 1971, and Crane and Blood, 1979] is given in Fig. 2.4.5. At azimuths of 279.5° and 282.5° more than one rain cell would be present in the earth-space path simultaneously. As the storm moves, the complex structure of rain cells will form, change and reform while the earth-space path "samples" the non-stationary behavior.

This azimuthal complexity, coupled with the non-uniform distribution with elevation and the small diameter-to-height ratios of typical intense rain cells, makes the determination of any elevation-angle dependence of path attenuation very difficult. Consequently, statistics gathered on path attenuation over long periods of a year or more ought to have a complex mixture of all forms of path and elevation-angle dependences. It seems likely, therefore, that such long-term statistics should show little or no elevation-angle dependence, and models for system availability taken from such statistical data should not show elevation-angle dependence[*].

2.5 <u>Some Observations on the Time Structure of Rain-Induced Fading</u>

Although the measures used in this report are based on 1-minute period rain rates, much more rapid fluctuations in point rain rates exist. Freeny and Gabe [1969] found rapid second-to-second fluctuations in fractional-second rain rates of up to 3 to 1 with 8-inch diameter "instantaneous" rain gauges. Since rain cells move at peak velocities of ~14 m/sec [Englebrecht, 1979][**]

---

[*]Much of the data used in this report was taken from radiometric sun-trackers and, therefore, represents a mixture of data from a continuum of elevation angles. Any elevation-angle dependence would not be retrievable.
[**]Average velocities are much lower, 1 to 4 m/sec [Crane, 1980].

TRANSVERSE DISTANCE AT 150 km (km)

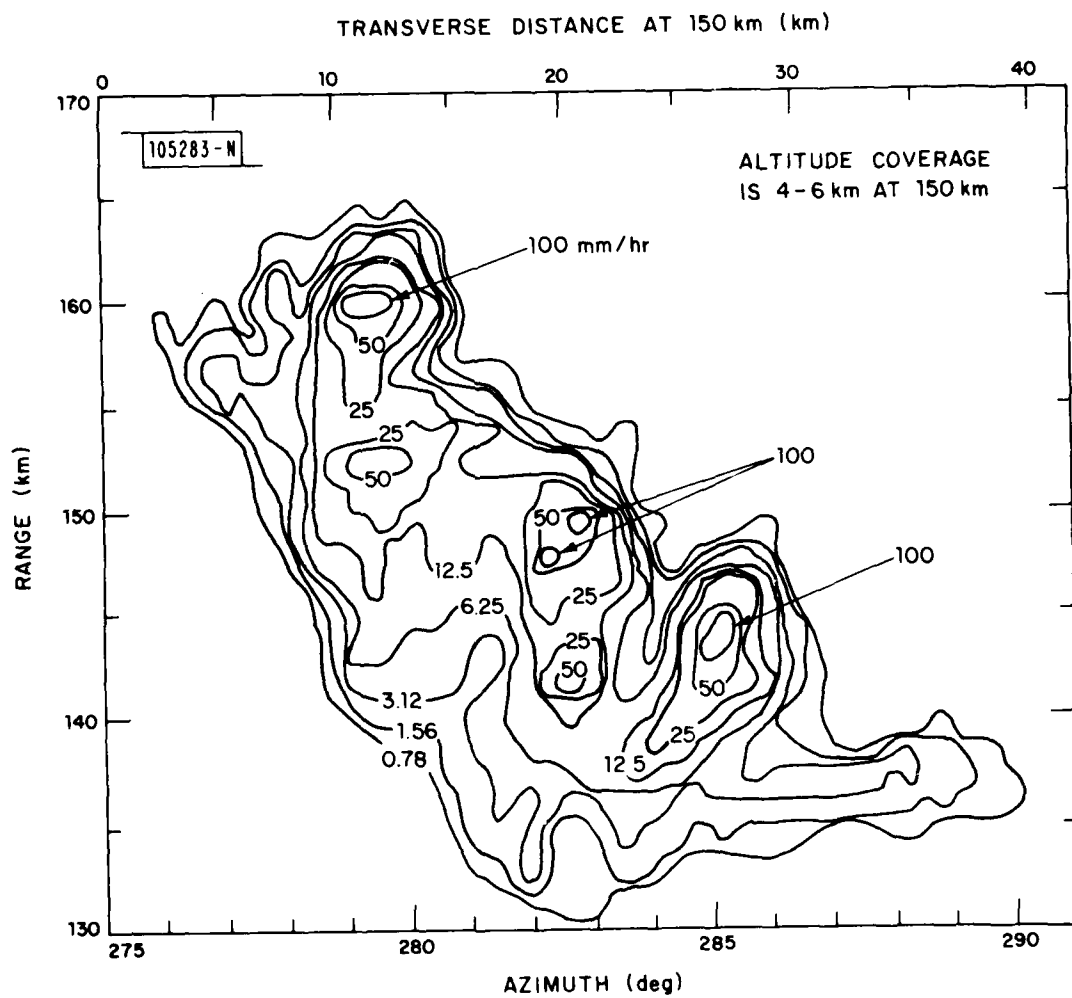ALTITUDE COVERAGE IS 4-6 km AT 150 km

105283-N

100 mm/hr

Fig. 2.4.5. Radar-derived range-azimuth cut at constant elevation angle (1.4°) through a thunderstorm.

and fine structure of the order of 1 m [Lin, 1975] in the cells can be moved by winds over 100 kms (~28 m/sec), such behaviors are to be expected. However, they are not necessarily representative of the path-integrated rain-rate behavior responsible for the total path attenuation at any given time.

On short-haul terrestrial paths of length L the effective volume of the path over which the rainfall will be averaged is the Fresnel ellipsoid of major axis L and minor axes $\sqrt{\lambda L}$ [Bodtmann and Ruthroff, 1974]. For an earth/satellite path, however, the effective averaging volume is encompassed by a paraboloid directed along the path as illustrated in Fig. 2.5.1. The height, h_o, of the melting layer and the elevation angle, θ, determine the effective rain-containing path length, L. The radius of the Fresnel zone is $\sqrt{\lambda L}$ and the volume is $\pi \lambda L^2/2$.

If h_o is set as the typical maximum height of the melting layer of 5 km (perhaps higher inside large thunderstorms) and $\theta=30^o$, the path length L=10 km. For a wavelength of 0.01 m (30 GHz), the Fresnel radius at the far end of the path is only 10 m and the volume is 1.57×10^6 m^3. For light rain of 0.25 mm/hr there are only about 20 drops/m^3 [Lin, 1975] and the number of drops in the Fresnel zone would only 3.14×10^7.

The averaging effect of the Fresnel zone, both in width and in length, restricts the time rate of change of attenuation. A "square" rain cell moving at 14 m/sec normal to the path would fill the path volume, if it were located near the melting height in the previous example, in about 0.7 second. Fine structure of the order of 1 m would transit the path in less than 1/4 of a second if being moved by 100-kph winds normal to the path. The fine structure would, however, contribute far less to the attenuation than would the cell itself. Consequently, the attenuation could be expected to change, in the worst case, several dB in a few seconds (1 to 3) with a low-level "noise" on the attenuation with spectral components constrained to the region of a few Hertz (1 to 5) or less[*].

---

[*]Their geometry would increase the attenuation "rise time" for cylindrical cells.
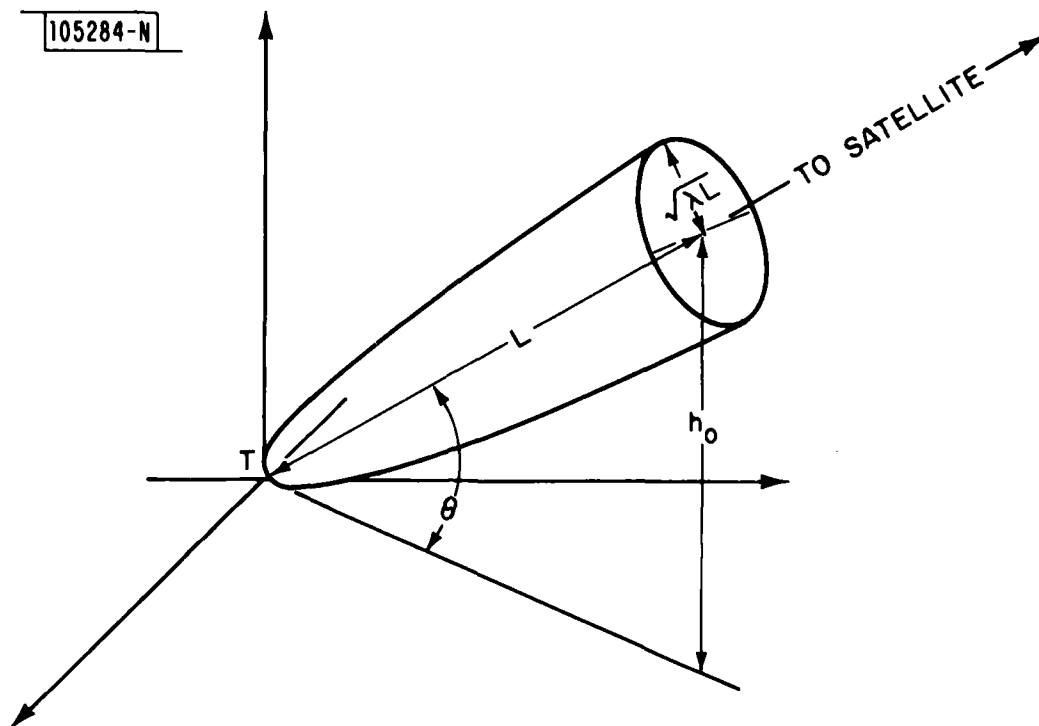
Fig. 2.5.1. First Fresnel zone for a terminal-satellite path of elevation angle, θ, to a melting layer height, h_o, with consequent effective path length, L.
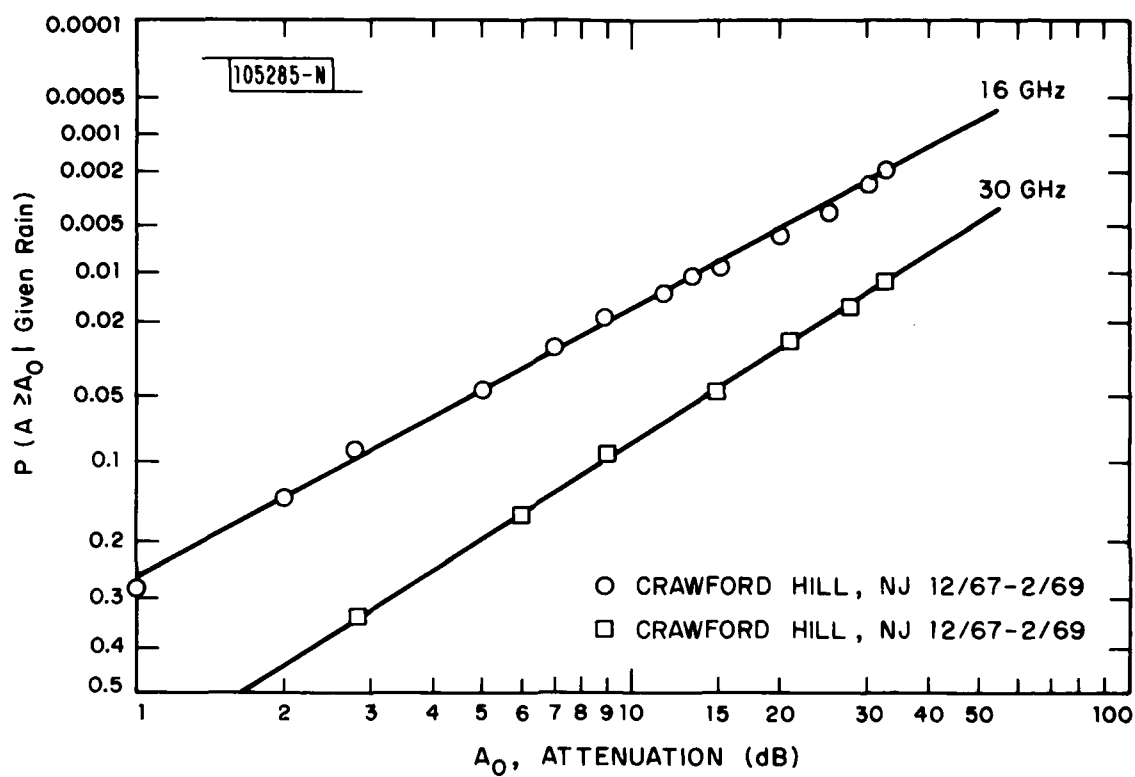
Fig. 2.6.2.1. Attenuation data for Crawford Hill, NJ.
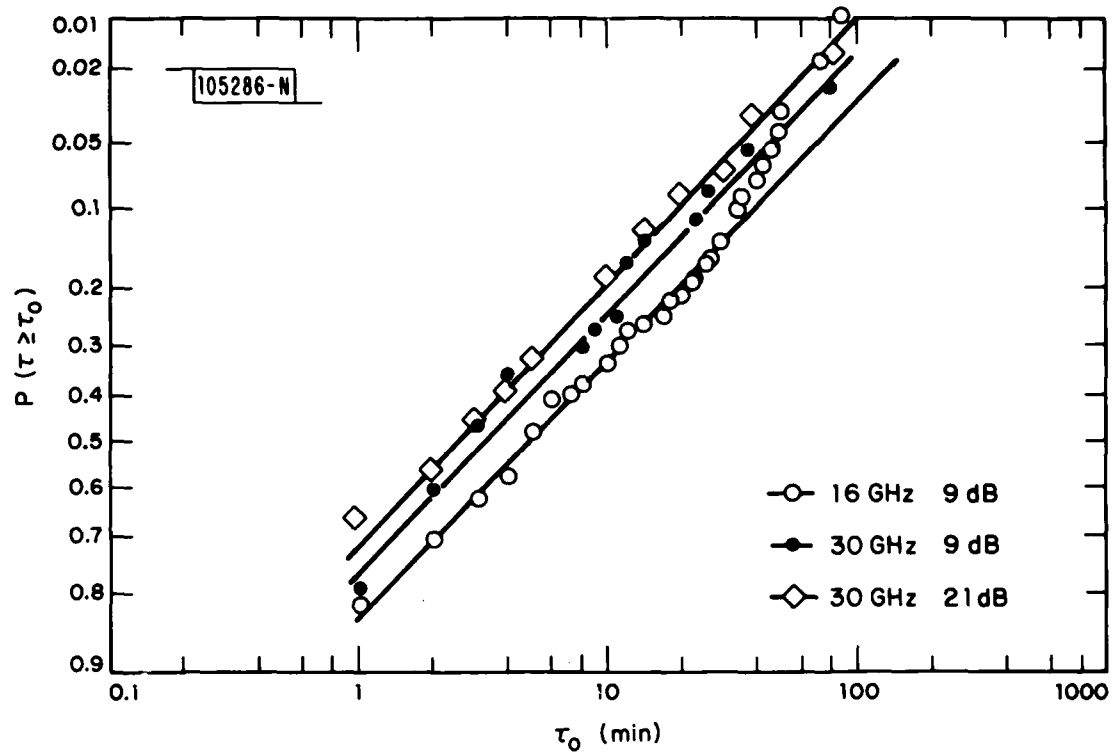
34

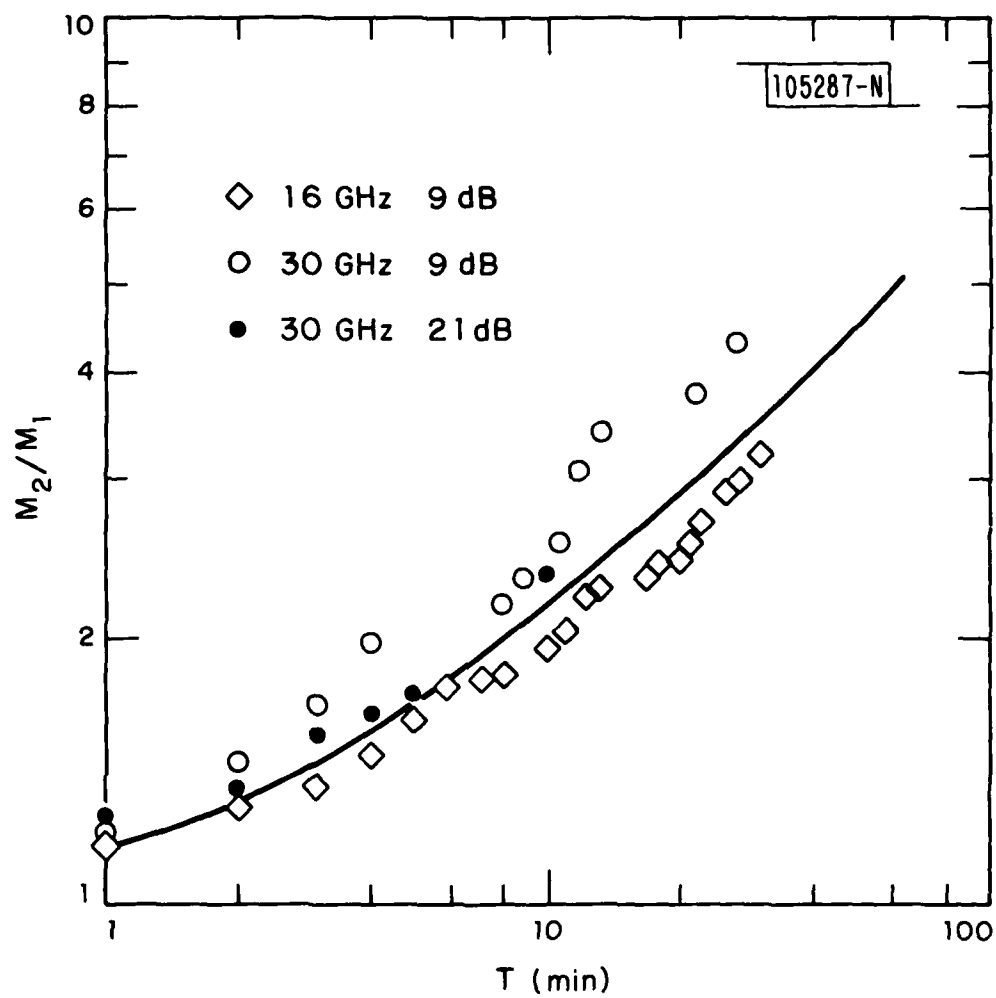Fig. 2.6.2.2.   Fade-duration distributions for Crawford Hill, NJ.

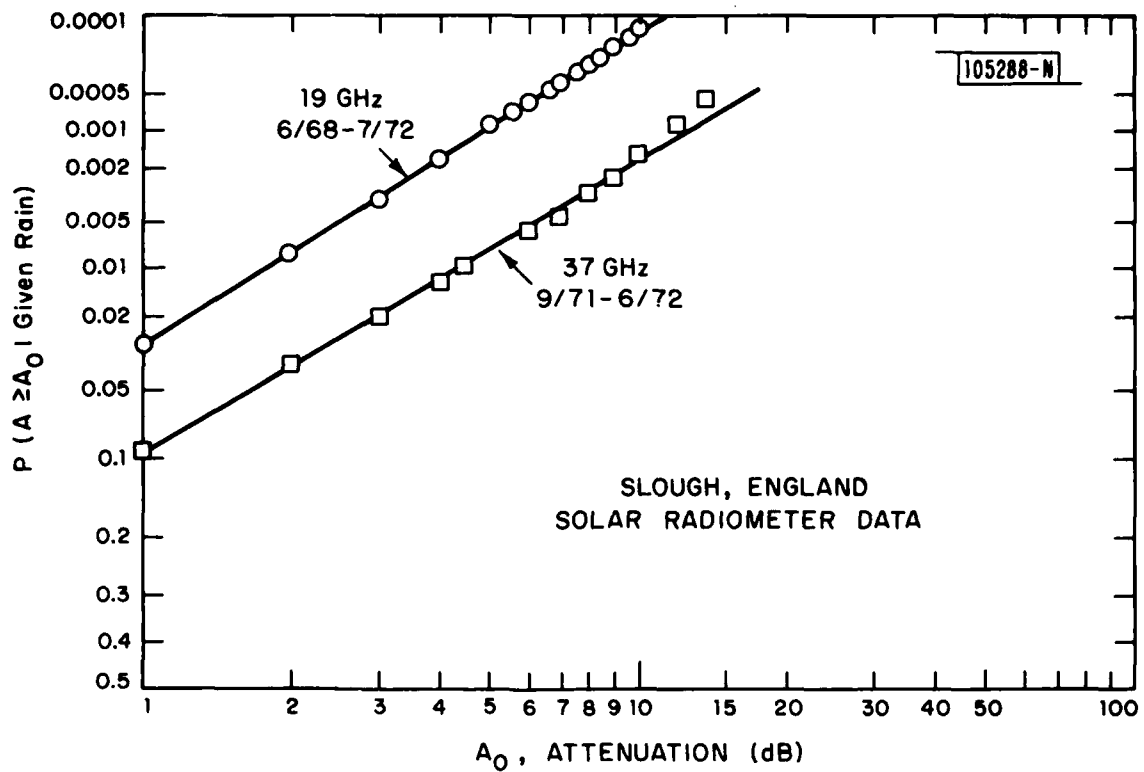Fig. 2.6.2.3. Margin Increase for Crawford Hill, NJ.
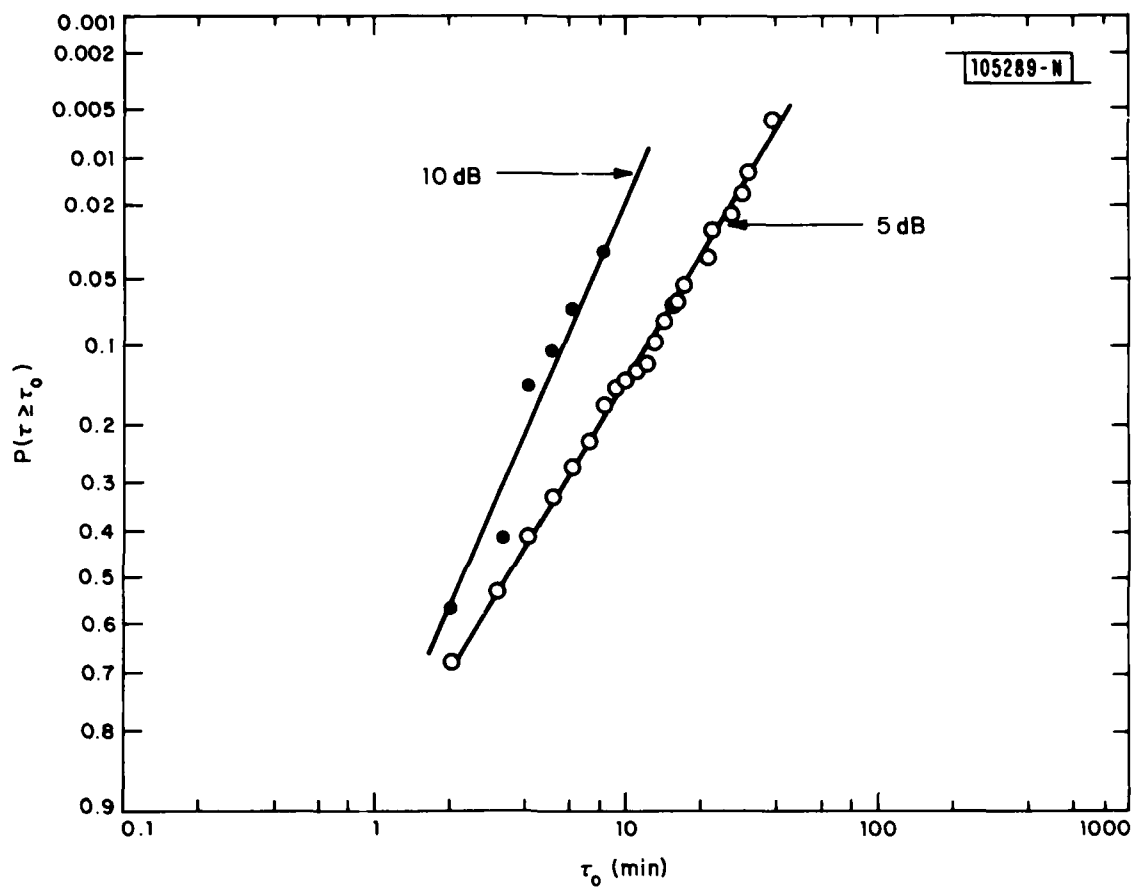
Fig. 2.6.3.1. Attenuation Data for Slough, ENG.

Fig. 2.6.3.2.   Fade-duration distributions for Slough, ENG, at 19GHz.
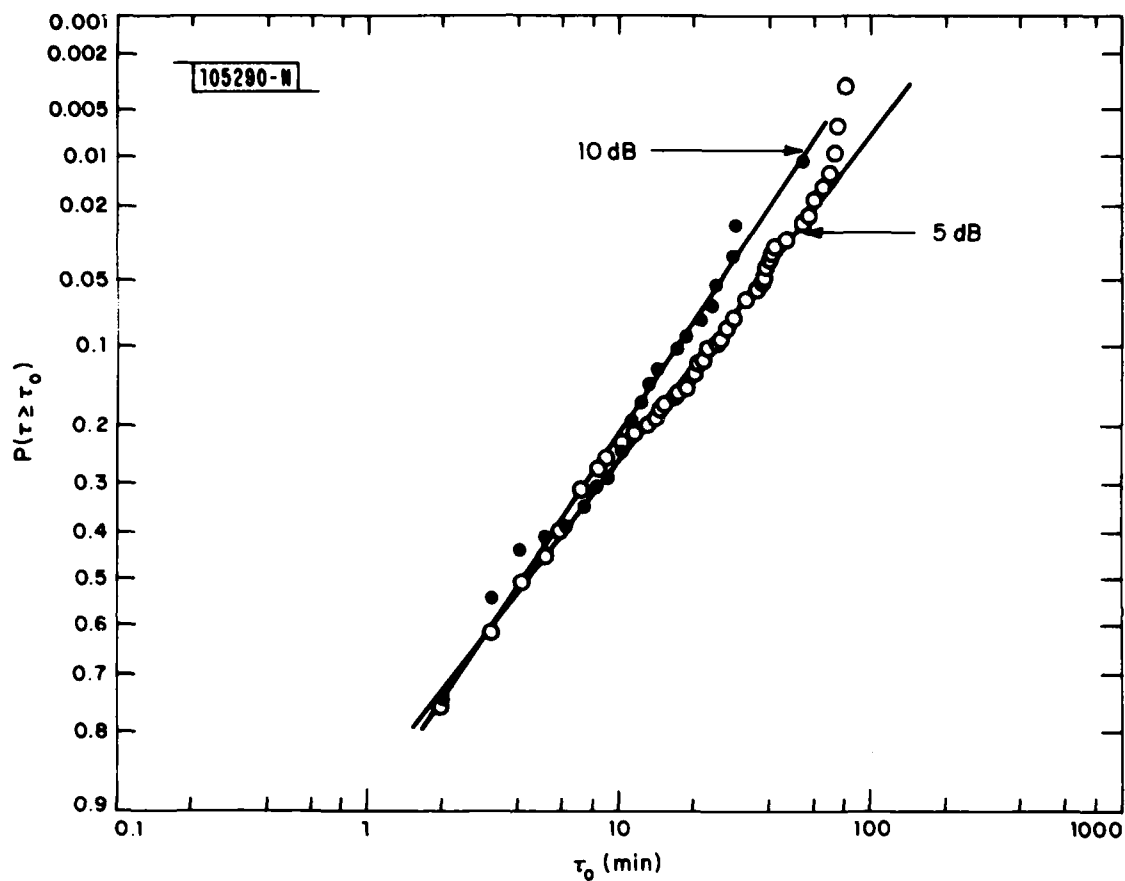
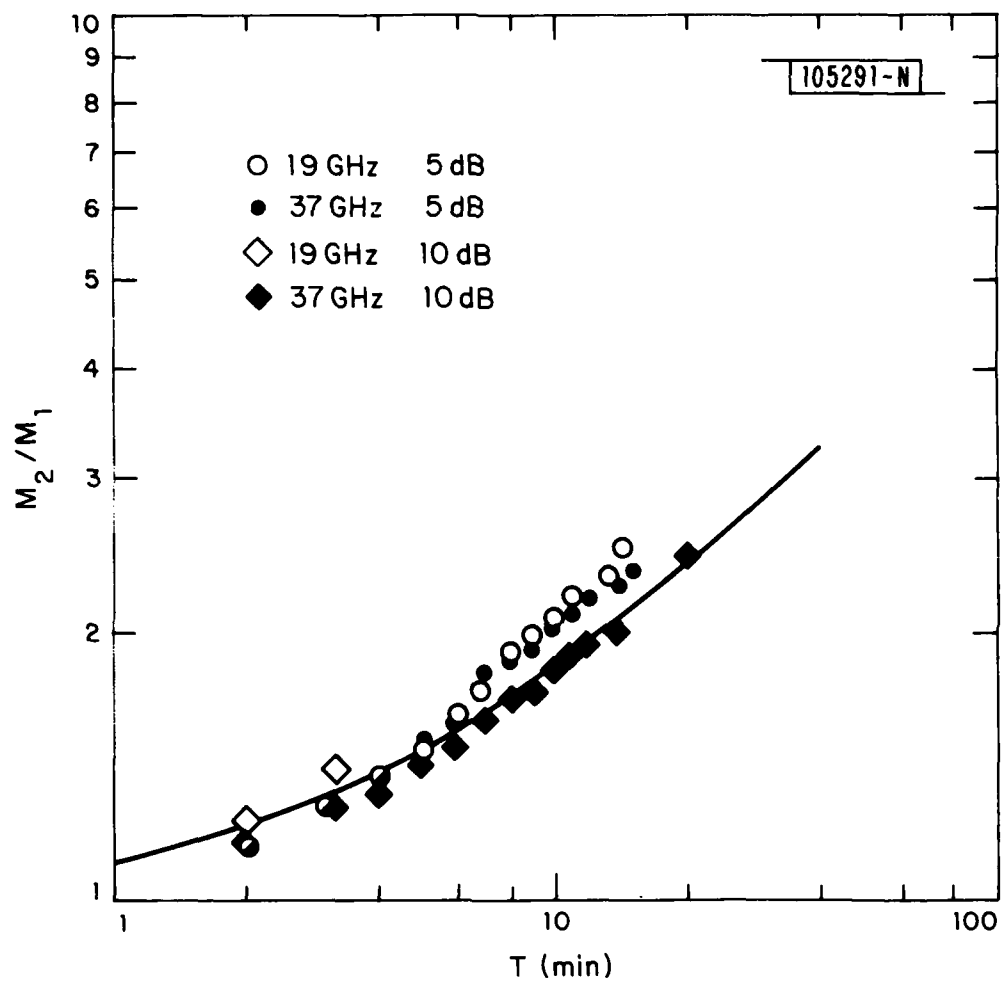Fig. 2.6.3.3.   Fade-duration distributions for Slough, ENG at 37 GHz.

Fig. 2.6.3.4. Margin increase for Slough, ENG.

40

From these numerical examples, it can be seen that the onset of rain-induced fades can be rapid, but not instantaneous. A few seconds should be available to sense the onset of the fade and to take corrective action. Although there will be fine structure on the attenuation with significant spectral components below a few Hertz, such fine-structure amplitude modulation should only affect those systems where significant carrier-to-noise ratios below a few Hertz from the carrier are required. It is interesting to note that these "rapid" fine-structure modulations would still only amount to a spectral spread of a few parts in 10^{11} at 30 GHz and would probably be overwhelmed by the short-term noise of the frequency standards used in the terminal and/or satellite.

Finally, some of the data used in this report was obtained from sun-track experiments. The sun is not a point source but instead occupies an angular extent of about 8.7 milliradians. At 30 GHz the 10-km Fresnel zone occupies an apparent angle of 2 milliradians. Therefore, the high frequency time structure of attenuation observed by a sun tracker might be expected to be somewhat different than that observed on a satellite downlink. This difference occurs for much the same reason that stars visibly "twinkle" under natural atmospheric turbulence but planets do not. Some additional averaging of path attenuation fluctuations is present, if the source has significant angular extent.

2.6 Model Inputs

2.6.1 Data Ordering

Each group of data from a given site and given frequency is reduced, if necessary, to the distribution function of attenuation when it is raining, with the aid of P_{RAIN} as determined in Section 2.3. From the $P(\tau > \tau_0)$ and the $P(A > A_0 | \text{given rain})$ the relation in (2.1.7) will give a value of M_2 for each M_1 and storage time, $T = \tau_0$. All of the data points are gathered together on one plot of M_2/M_1 versus T.

The points on the individual plots of M_2/M_1 versus T are fitted to the empirical relation

$$M_2/M_1 = (1 + \frac{T}{T_o})^{0.5} \qquad\qquad (2.6.1.1)$$

with the value of T_o chosen to give the best mean-square-error fit to the data. It is interesting to note that, with few exceptions, the data points on the M_2/M_1 versus T plots show little or no variation with M_1 or operating frequency. There does appear to be a variation in T_o from site to site, however. The reasons for such variation will be examined in Section 2.7.

2.6.2   Crawford-Hill, NJ, Data

Sun-tracker experiments were carried out by Bell Telephone Laboratories at Crawford Hill, NJ, from 12/67 to 2/69 [Wilson, 1969, and Lin, 1973]. The 16-GHz and 30-GHz distribution functions for $P(A \geq A_o | \text{given rain})$ are given in Fig. 2.6.2.1 and the distribution functions for duration of fade, $P(\tau \geq \tau_o)$, for 9-dB and 21-dB thresholds at 30 GHz and a 9-dB threshold at 16 GHz are given in Fig. 2.6.2.2.

It is interesting to note that the data presented in Figs. 2.6.2.1 and 2.6.2.2, plotted on "log-normal-straightening" paper, fit straight lines rather well. The only exception appears at the long durations at the lowest frequency. Such deviations are to be expected in a finite data set [Lin, 1976b], where the tails of the distributions would not be expected to be precisely lognormal.

The generated plot of M_2/M_1 versus T is given in Fig. 2.6.2.3. A value for T_o of 2.6±0.7 minutes fits the data best and the resulting curve of (2.6.1.1) is given on the same figure.

2.6.3   Slough, ENG, Data

Sun-tracker experiments were carried out by the GPO at Slough, ENG, at 19 GHz from 9/68 to 7/72 and at 37 GHz for the rather brief period of 9/71 to 6/72 [Davis, 1971, and Davis, 1973]. The resulting curves of $P(A \geq A_o | \text{given rain})$ are given in Fig. 2.6.3.1. Fade-duration distributions for 5-dB and 10-dB thresholds at 19 GHz are given in Fig. 2.6.3.2 and at 38 GHz in Fig. 2.6.3.3.

Again, a good fit to lognormal distributions, except at the extreme tails, is noted. The data points in Fig. 2.6.3.4 for M_2/M_1 versus T are surprisingly tight and well-fitted by T_o=4.15±0.97 minutes.

2.6.4   Rosman, NC, Data

Satellite-link experiments were carried out at 30 GHz from the NASA site at Rosman, NC [Ippolito, 1975, and Crane, 1980]. The period covered only a few of the months (summer) of 1974 so the data are not expected to be a good representation of a year-long sample. However, $P(A > A_0 |$given rain) is plotted in Fig. 2.6.4.1 and the fade-duration distributions for 5-dB, 10-dB and 15-dB thresholds are given in Fig. 2.6.4.2.

The resulting M_2/M_1 behavior versus T is given in Fig. 2.6.4.3. As expected, the scatter is large and the rather loose fit is also implied by a value of $T_0 = 1.42 \pm 1.17$ minutes.

2.6.5   Waltham, MA, Data

Satellite-link experiments using CTS were carried out at 11.7 GHz at Waltham, MA, over the two periods 2/77 to 1/78 and 2/78 to 1/79 [Nackoney, 1979, and Tang, 1979]. The resulting $P(A > A_0 |$given rain) is given in Fig. 2.6.5.1. Fade-duration distributions for 3-dB, 6-dB and 10-dB thresholds are given in Fig. 2.6.5.2. The M_2/M_1 versus T plot of Fig. 2.6.5.3 yields a value of $T = 2.08 \pm 1.53$ minutes.

Note that the two years of data in Fig. 2.6.5.1, if separated, show distinct abnormalities at the low-probability/high-attenuation end of the curves. The period 2/78 to 1/79 deviates significantly from lognormal in such a fashion that high attenuation events would be expected to be more rare for that period than for 2/77 to 1/78. In fact, as shown in Table 2.3.2 in Section 2.3, the number of thunderstorm days for the period 2/78 to 1/79 is 11, one-half of the value of 22 for 2/77 to 1/78 and about one-half of the average value of 19. Therefore, the lack of a normal number of high-attenuation events for the period 2/78 to 1/79 is expected; however, the average of 19 thunderstorm days for the two-year period is close to nominal and the composite data is consequently close to the expected lognormal behavior.

2.6.6   Austin, TX, Data

The 11.7-GHz signal from the CTS satellite was also used to gather attenuation data at Austin, TX, for the period 2/78 to 1/79. The plot of $P(A > A_0 |$given rain) is illustrated in Fig. 2.6.6.1 and 3-dB, 6-dB and 10-dB
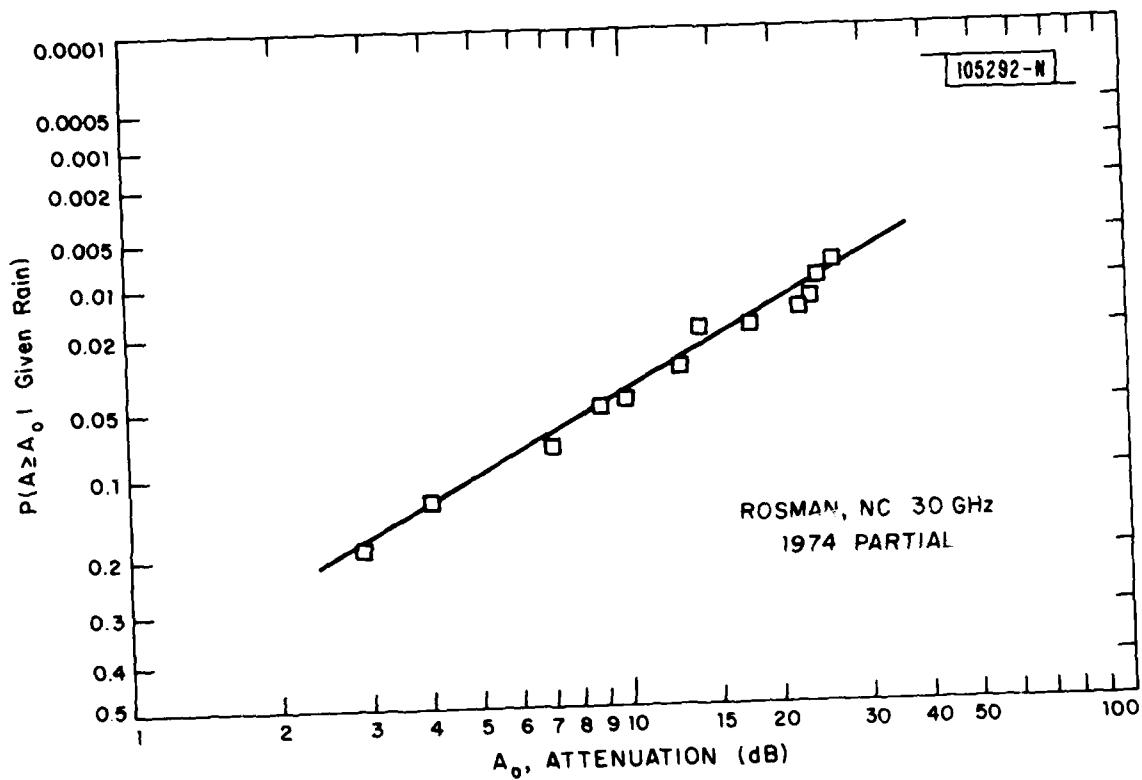
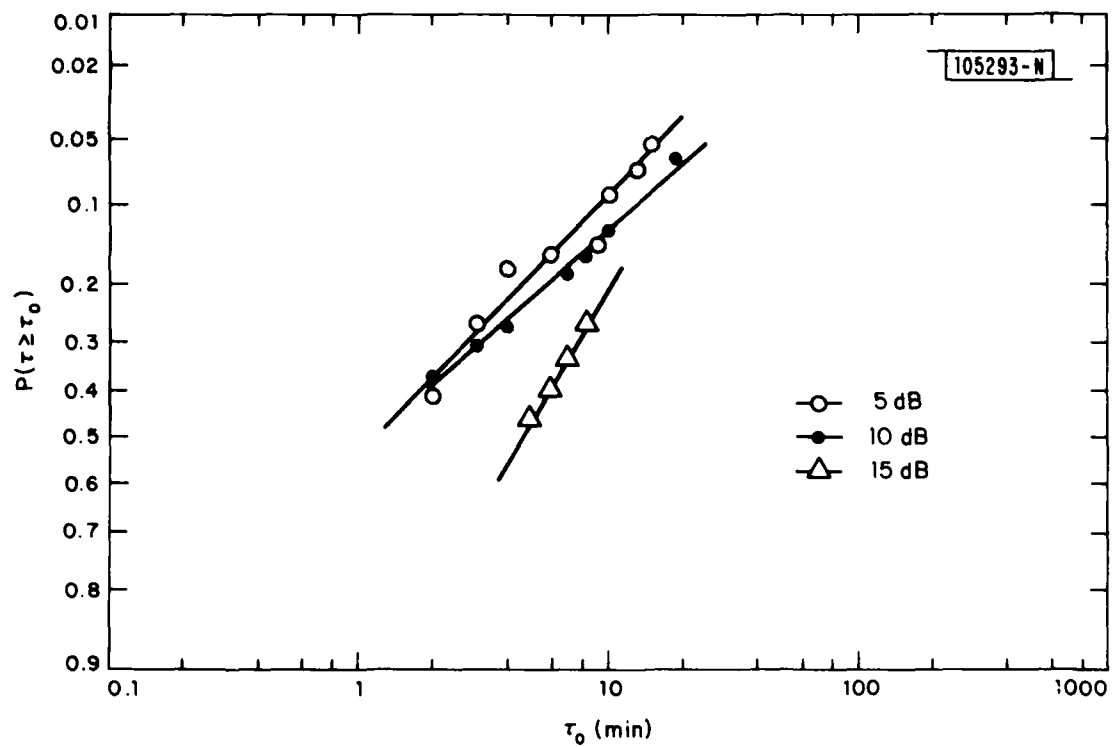Fig. 2.6.4.1. Attenuation data for Rosman, NC.

44

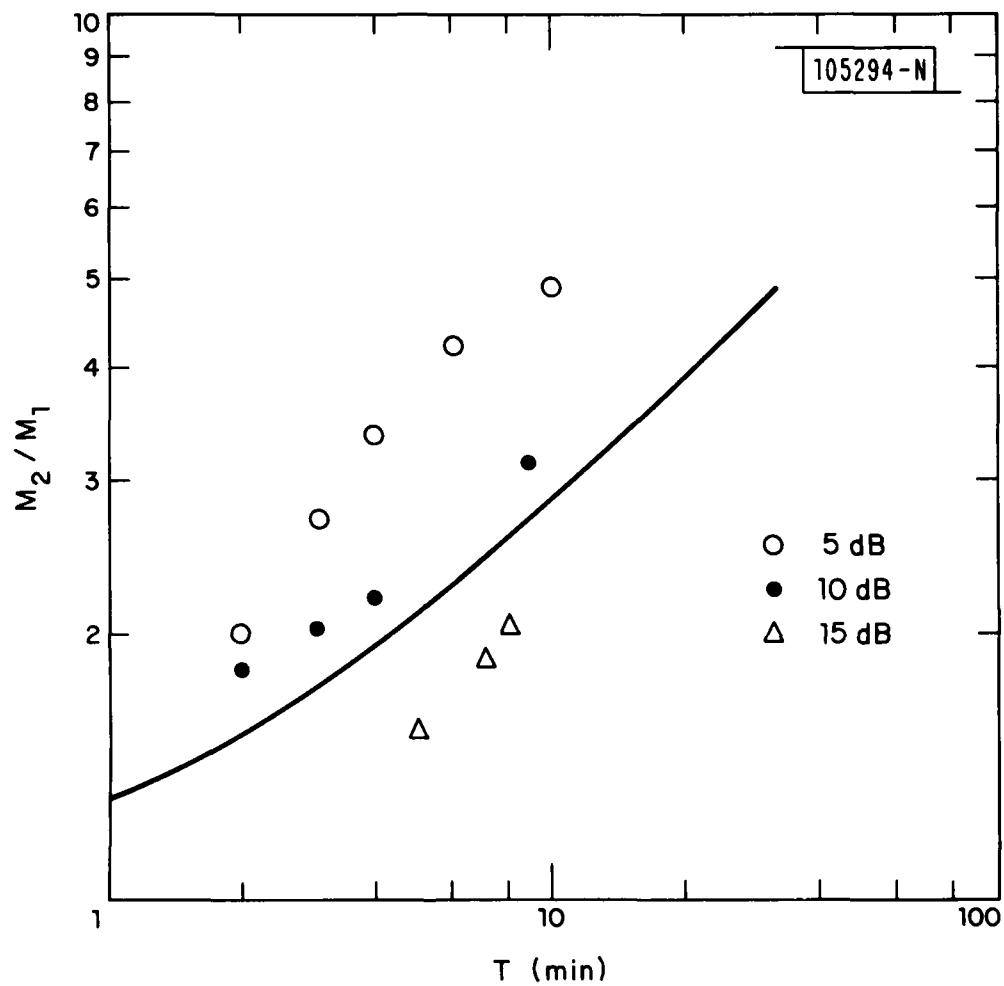Fig. 2.6.4.2. Fade-duration distributions for Rosman, NC.

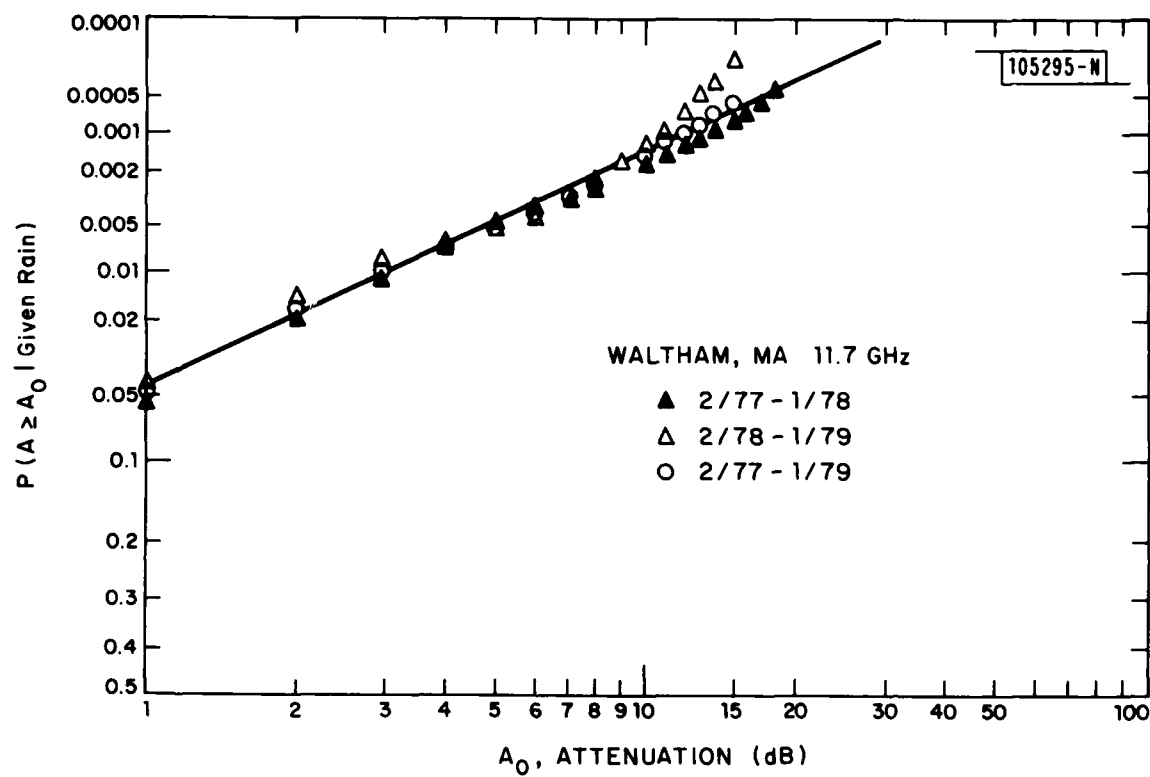Fig. 2.6.4.3. Margin increase for Rosman, NC.
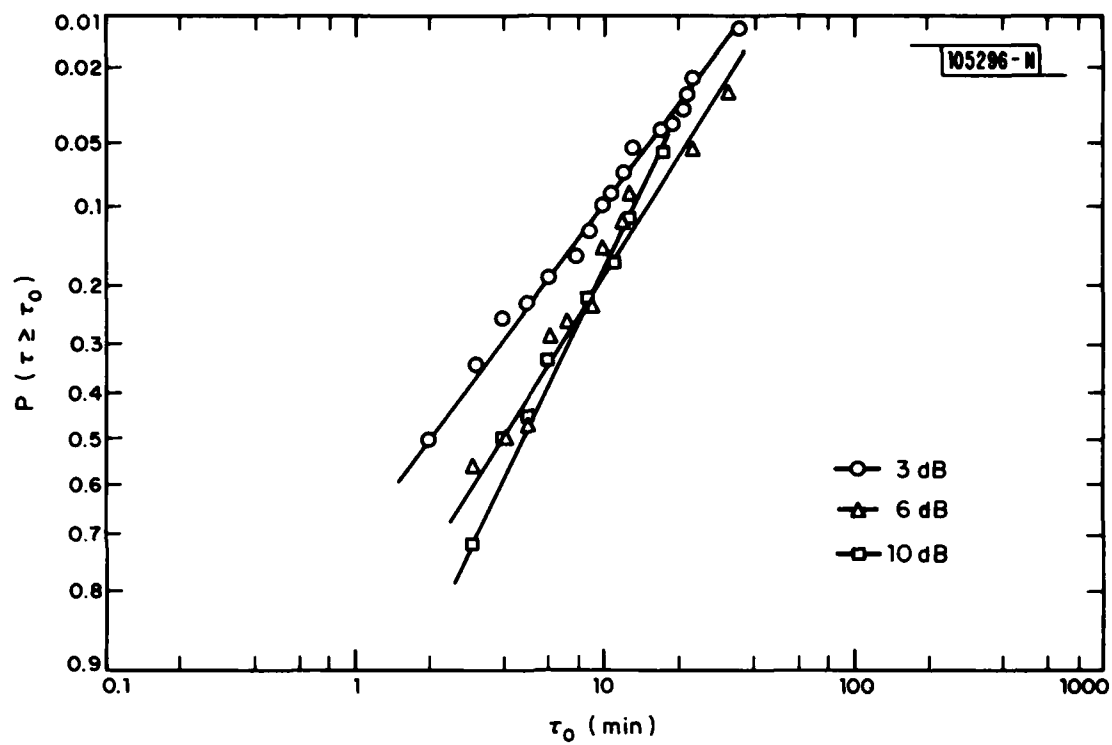
Fig. 2.6.5.1. Attenuation data for Waltham, MA.

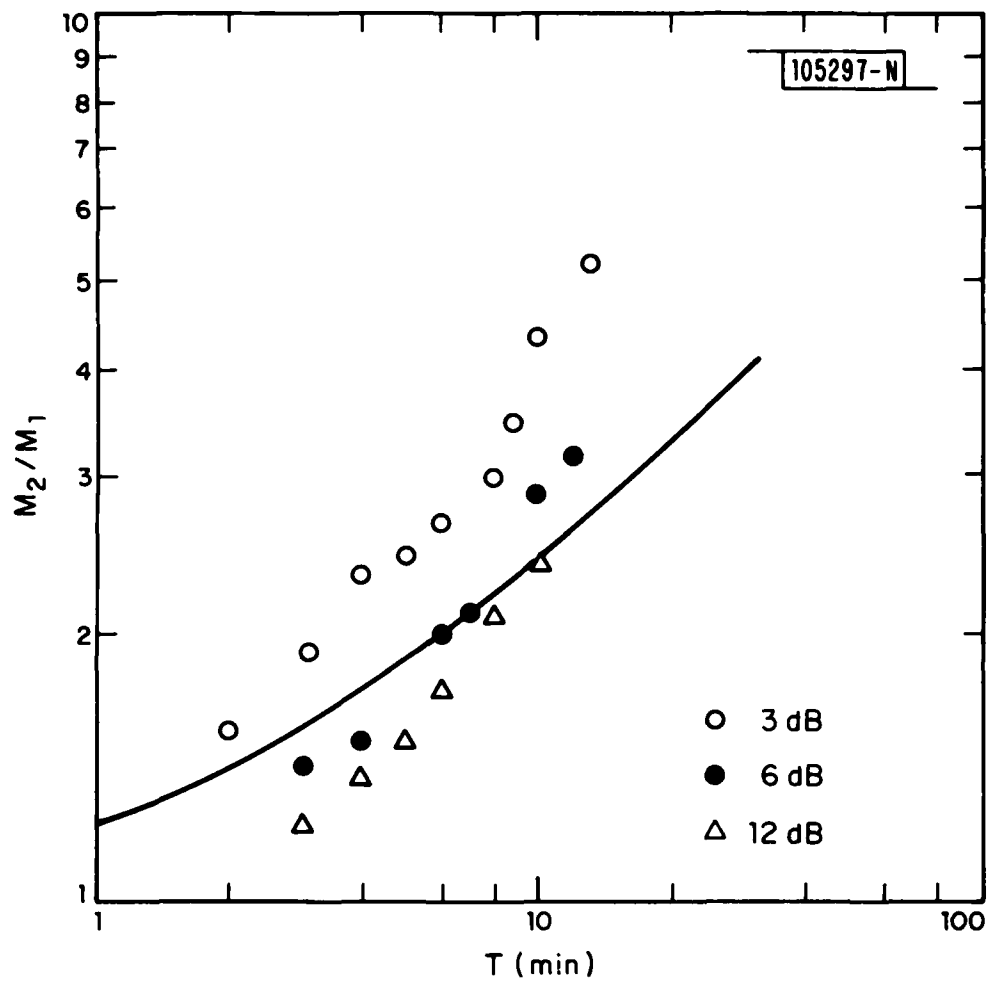Fig. 2.6.5.2. Fade-duration distributions for Waltham, MA.

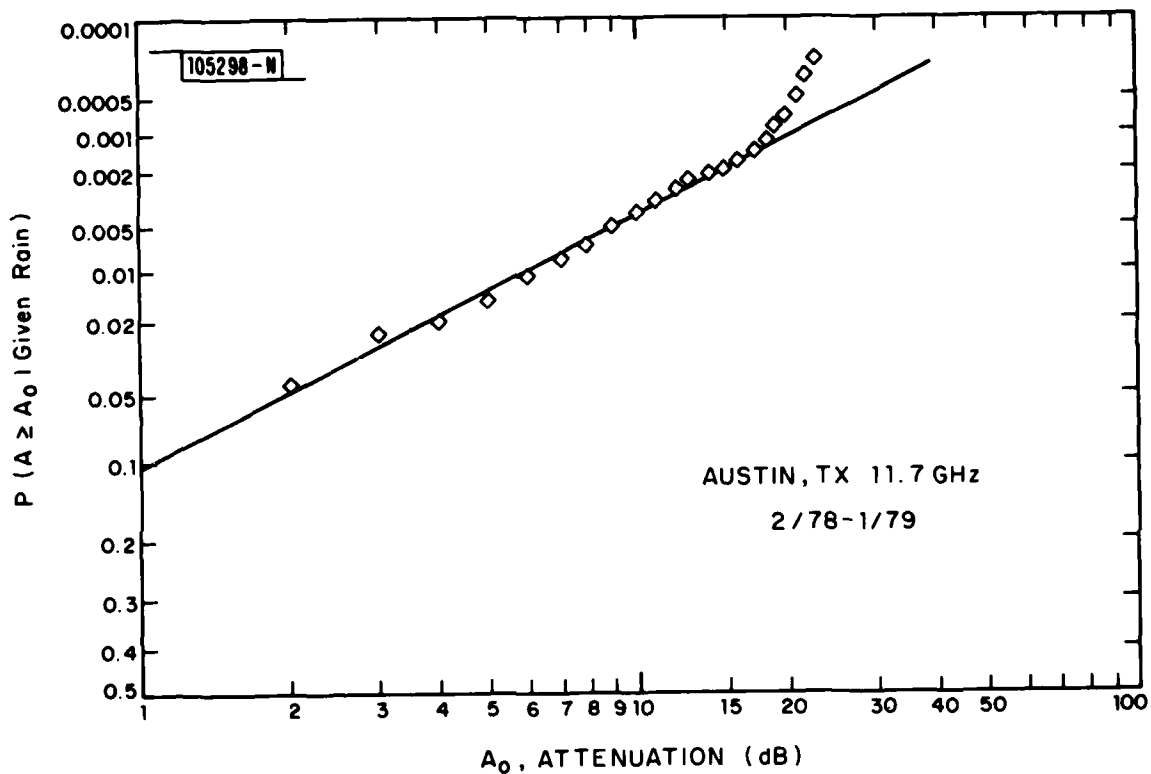Fig. 2.6.5.3. Margin increase for Waltham, MA.

49

Fig. 2.6.6.1. Attenuation data for Austin, TX.

50

threshold fade-duration distributions are given in Fig. 2.6.6.2. A value of $T_o = 1.85 \pm 0.63$ minutes is indicated by the M_2/M_1 versus T behavior in Fig. 2.6.6.3.

As in the second year of the Waltham, MA, data, there is a significant lack of high-attenuation events in the Austin, TX, data. From Table 2.3.2 the number of thunderstorm days for the observing period was only 17, less than one-half the nominal value of 41. Therefore, the period was abnormal and a data take over several years would be expected to have a better distribution in the tails.

2.6.7   Tampa, FL, Data

Data were taken over the period 1/78 to 12/79 using the COMSTAR 19-GHz beacon at 3 sites in the Tampa, FL, area [Tang, 1979, and Tang, 1980]. The complete attenuation data for the University of Southern Florida (USF) site were supplied by Tang [1980] as a personal communication and are plotted in Fig. 2.6.7.1. The fade-duration data are given for 6-dB and 12-dB thresholds in Fig. 2.6.7.2.

The fade-duration data exhibit a strange behavior at both the "low-probability" tails and the "high-probability" tails. The deviations at the low-probability extreme tails can be explained on the basis of a limited sample of data. The high-probability anomaly is a different matter. It is not clear if it results from an instrumentation or computational "glitch" or if it is real[*].

Because of this anomaly two different M_2/M_1 versus T data sets are presented in Fig. 2.6.7.3. One, termed "actual", follows the data points in Fig. 2.6.7.2. The second, termed "projected" follows the projected lognormal behavior in Fig. 2.6.7.2. There are, therefore, two values of T_o, a "projected" value of $T_o = 0.43 \pm 0.13$ minute and an "actual" value of $T_o = 0.29 \pm 0.05$ minute.

---

[*]If there were a slow-response problem in the amplitude-measuring equipment, the shorter fades might well be "filled in" and missed.
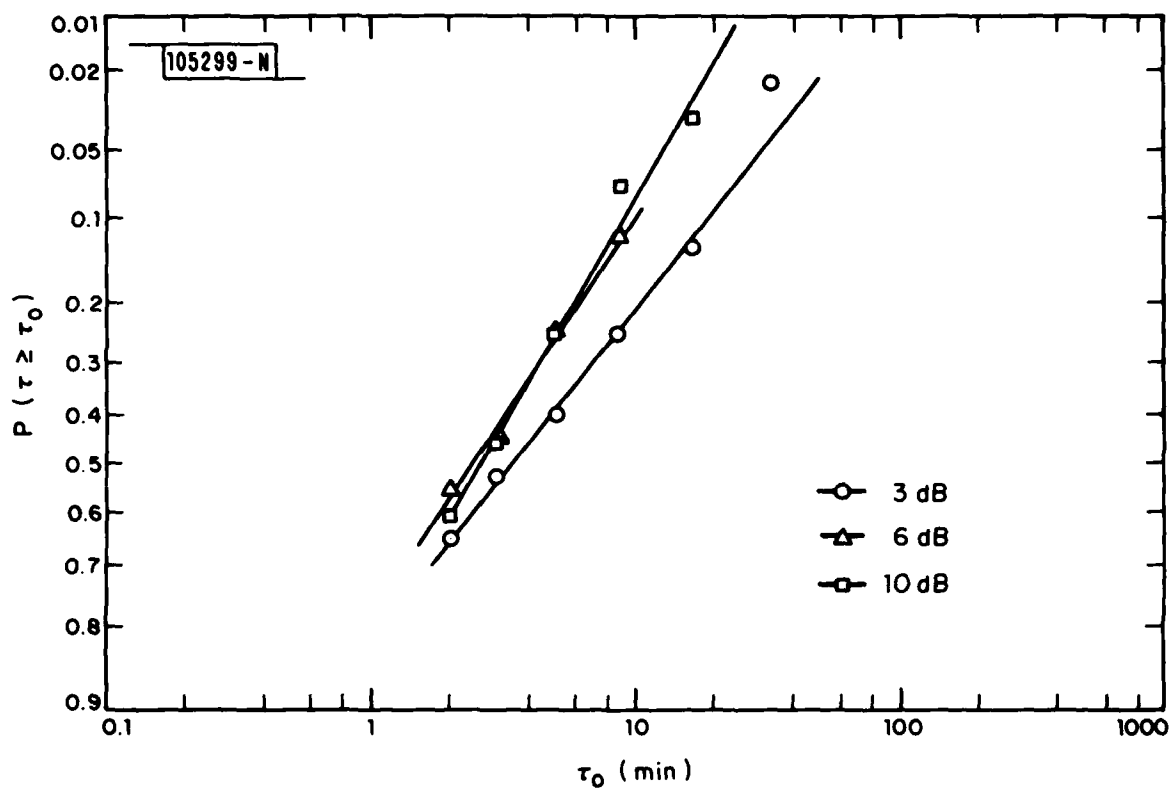
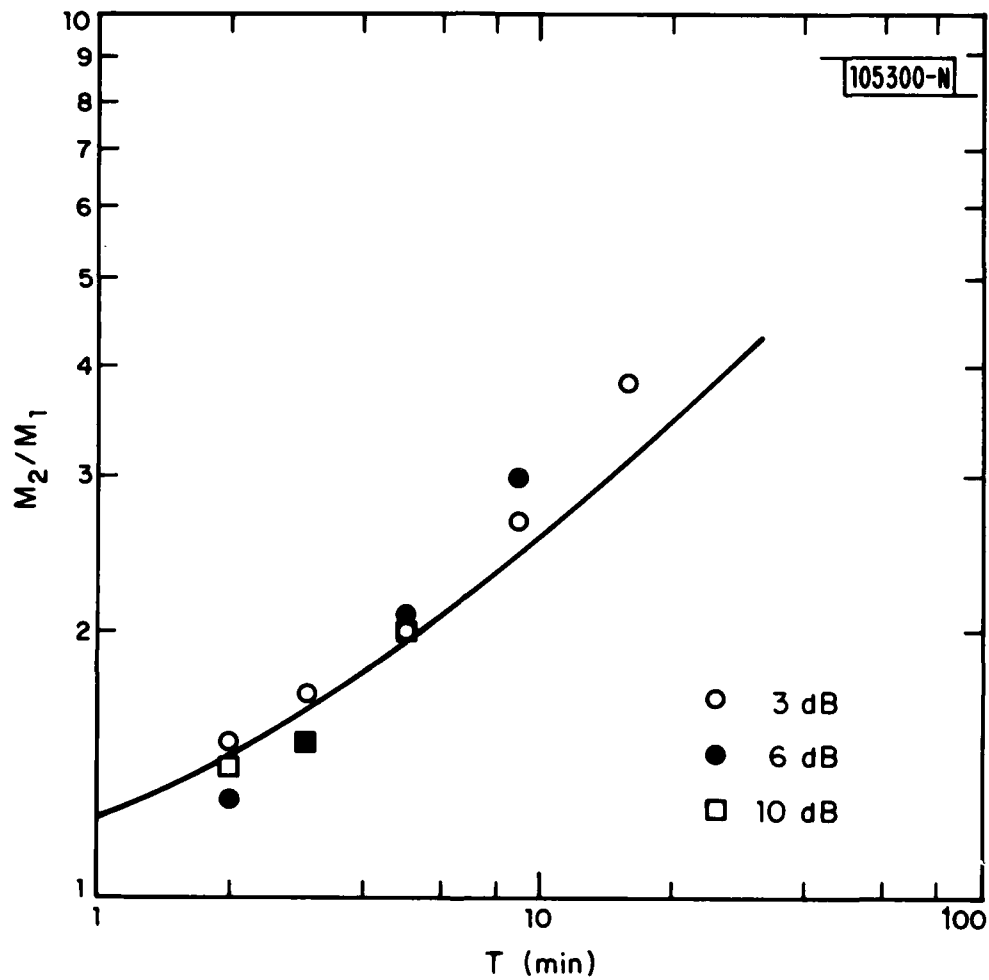Fig. 2.6.6.2. Fade-duration distributions for Austin, TX.

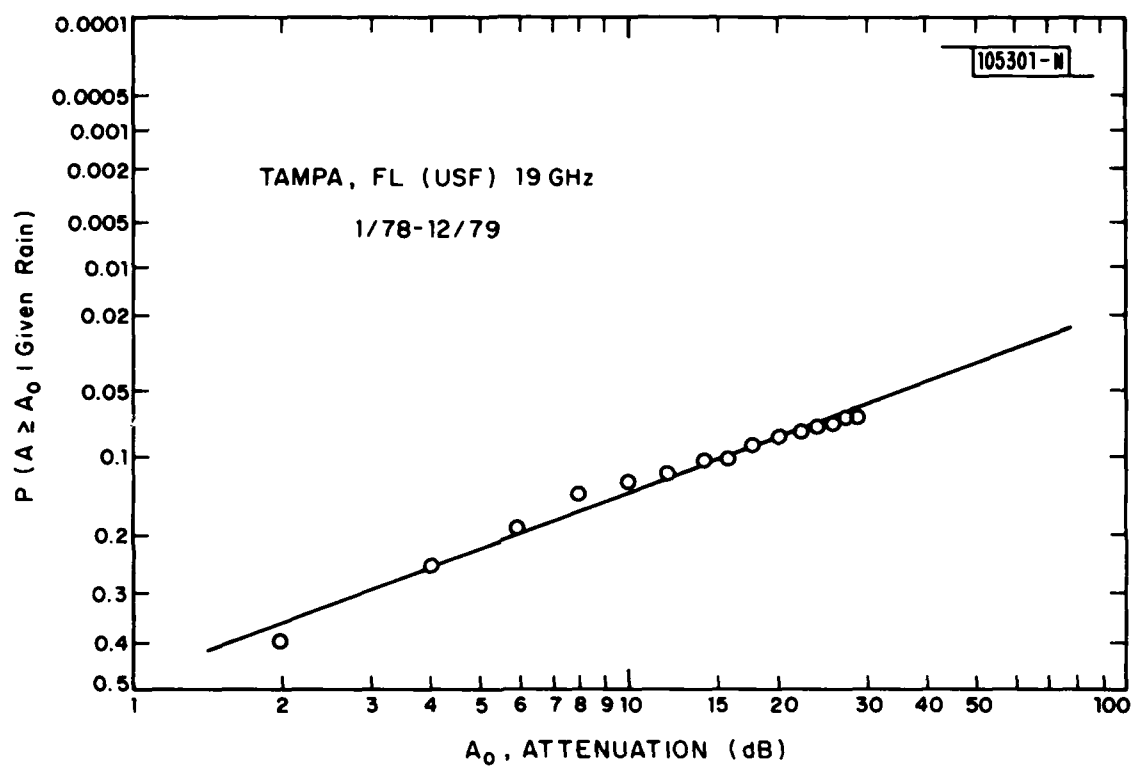Fig. 2.6.6.3. Margin increase for Austin, TX.
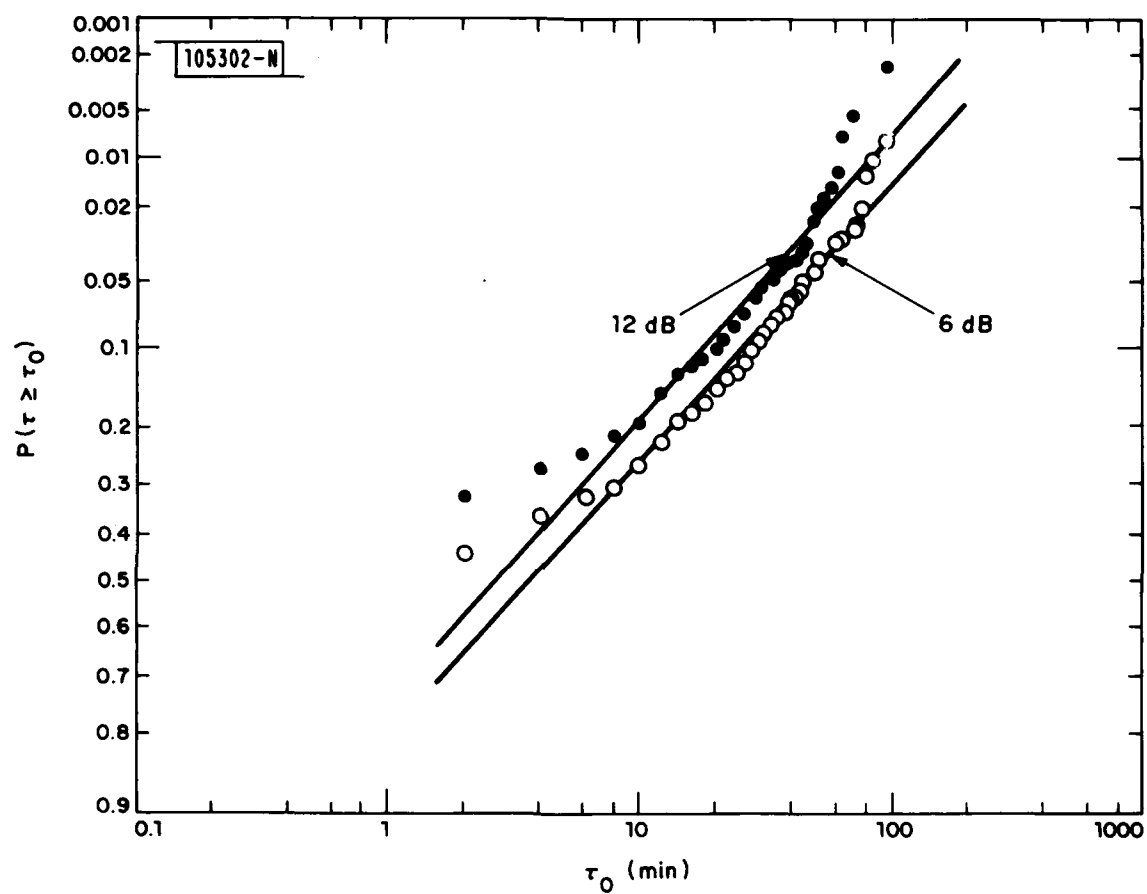
Fig. 2.6.7.1. Attenuation data for Tampa, FL.
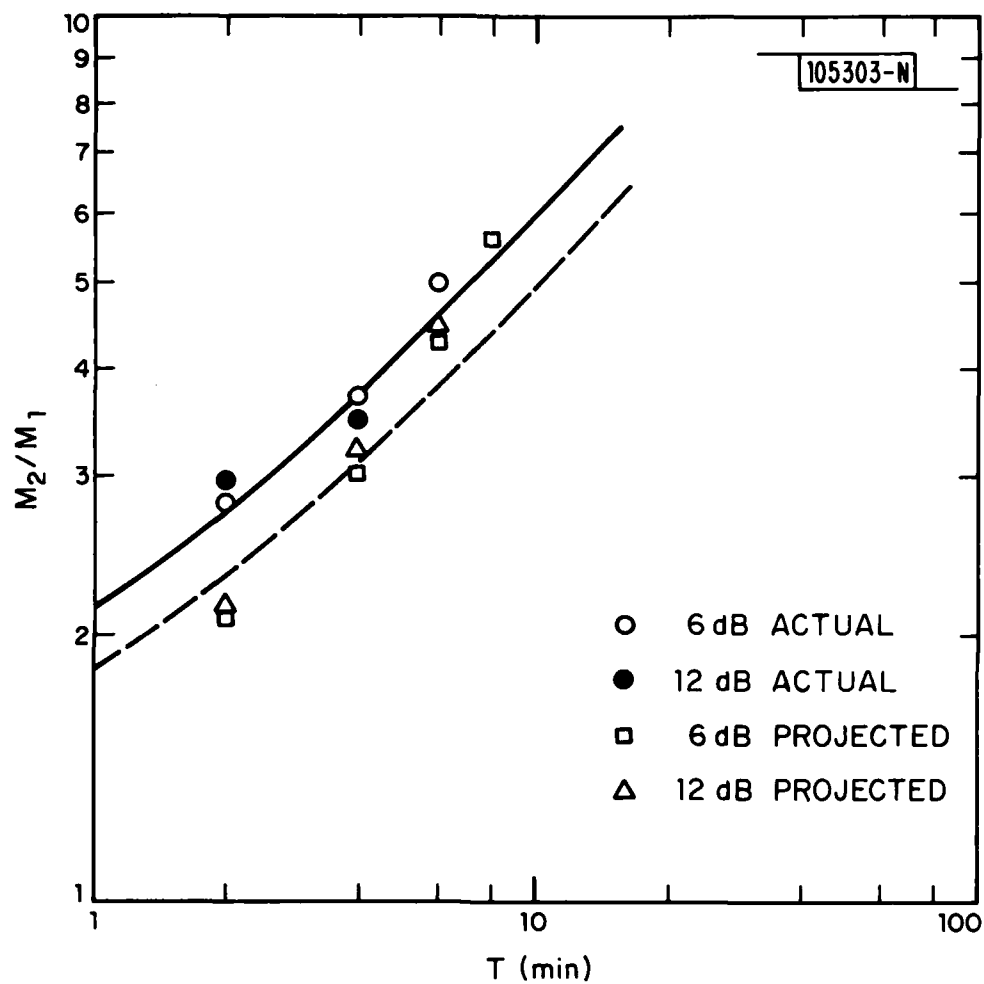
Fig. 2.6.7.2. Fade-duration distributions for Tampa, FL.

Fig. 2.6.7.3. Margin increase for Tampa, FL.

2.7 A Storage-Time Model

Each of the data sets from different locations was analyzed in Section 2.6 and a storage-time relationship of the form

$$M_2/M_1 = [1 + \frac{T}{T_o}]^{0.5} \tag{2.7.1}$$

was derived for each location. The values of T_o, however, varied from a low of 0.43 minute in Tampa, FL, to a high of 4.15 minutes in Slough, ENG. It remains to determine if certain climatological factors can be identified as the causes of this nearly ten-to-one change in the parameter T_o.

The characteristics of rainfall from thunderstorms are dominated by short-duration high-rate events, whereas the more widespread rainfall is more likely to have long-duration moderate-rate events. Therefore, it should be expected that the storage-time requirements for Tampa, FL, where much of the rainfall is from thunderstorms, would be less than those for Slough, ENG, where most of the rainfall is not thunderstorm-derived. As noted in Section 2.3, a useful index is the ratio of thunderstorm days to days of measurable precipitation, D_T/D_R.

Values of D_T/D_R for the periods of time and locations are taken from Section 2.3 and paired with the T_o values from Section 2.6 in Table 2.7.1. There are, of course, many different function behaviors for $T_o(D_T/D_R)$ that can be proposed. However, by plotting $\log T_o$ versus D_T/D_R in Fig. 2.7.1, a simple straight-line model can be deduced.

The model agreement is improved somewhat by realizing that the sun-tracker experiments at Crawford Hill, NJ, and Slough, ENG, typically do not operate when the sun is less than 20° above the horizon. Consequently, they will miss the early-evening and night-time population of thunderstorms. It is somewhat arbitrarily assumed that roughly one-third of the thunderstorms will be missed by such operation and the effective value of D_T/D_R will be reduced to two-thirds of its original value. Such a reduction is shown by the "dashed" circles in Fig. 2.7.1.

57

TABLE 2.7.1

VALUES OF T_o AND THUNDERSTORM INDEX, D_T/D_R FOR THE VARIOUS LOCATIONS

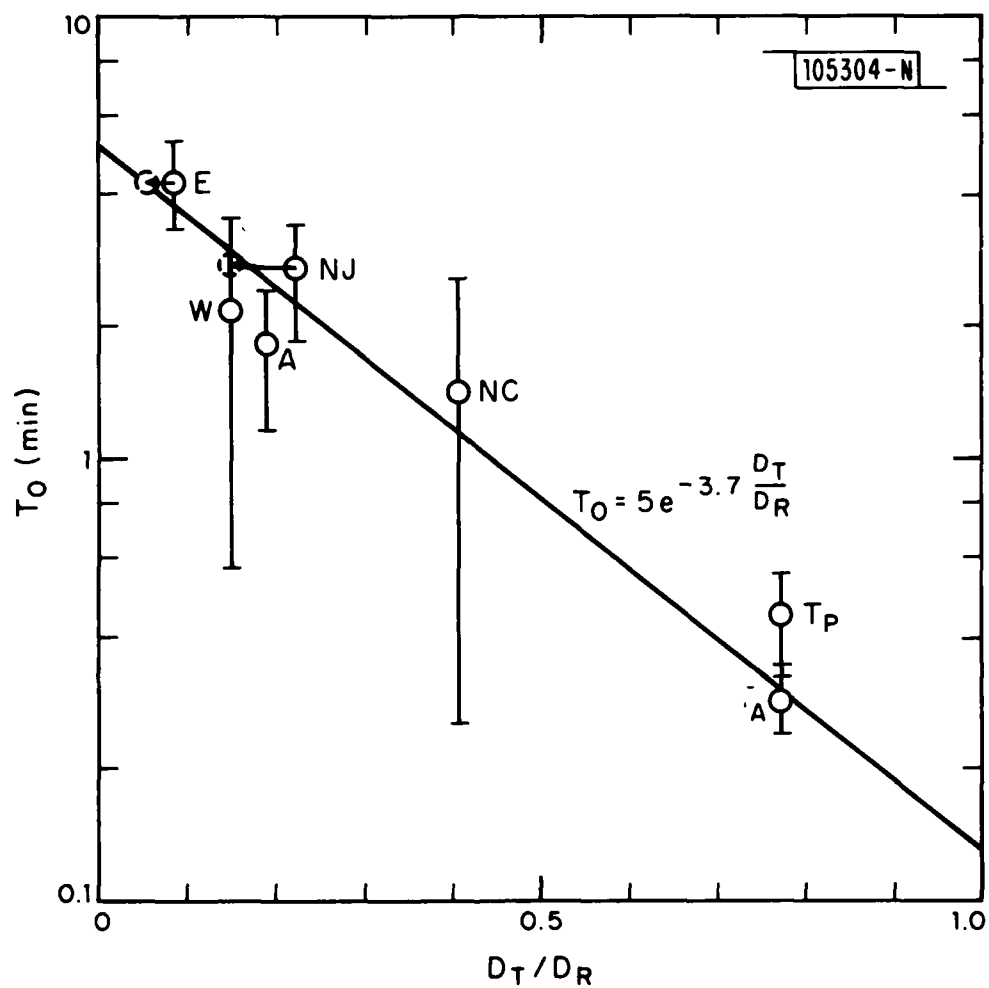| LOCATION	D_T/D_R		T_o, minutes
Crawford Hill, NJ	0.226		2.6 ± 0.7
Slough, ENG	0.088		4.15 ± 0.97
Rosman, NC	0.409		1.42 ± 1.17
Waltham, MA	0.149		2.08 ± 1.53
Austin, TX	0.191		1.85 ± 0.63
Tampa, FL	0.766	(actual)	0.29 ± 0.13
		(projected)	0.43 ± 0.05

Fig. 2.7.1. Storage-time normalizer, T_o, versus the thunderstorm index, D_T/D_R.

59

From Fig. 2.7.1, the model value for T_0 is

$$T_o = 5e^{-3.7D_T/D_R} \quad \text{minutes} \tag{2.7.2}$$

giving a storage-time relation of

$$M_2/M_1 = \left[1 + 0.2T \; e^{3.7D_T/D_R}\right]^{0.5} \tag{2.7.3}$$

Since $1 > D_T/D_R > 0$, the relationship in (2.7.3) is bounded so that climate areas like the Northwest coast of the US with D_T/D_R 0 and other areas like equatorial Africa and equatorial South America with D_T/D_R 1 are both represented. There is, therefore, some reason to believe that, within the limits of the data, the empirical storage-time model for (2.7.3) is geographically universal.

Finally, some measure of the scatter in the data can be determined by plotting M_2/M_1 versus the normalized storage time, T/T_o, for all of the locations on one graph. Such a plot is given in Fig. 2.7.2. Note that the four anomalous points on the low side of the composite come from the 15-dB threshold values for Rosman, NC, and represent an inadequate data base. There is also some reason to believe that threshold values of 3 dB or less do not yield good results. The 3-dB threshold points from various locations represent many of the widely scattered anomalous points on the high side of the composite curve. With such "bad" data excluded, over a range of $6 > M_2/M_1 > 1$, the required value of T/T_o determined directly from the data is less than a factor of 1.5 different than the predicted (model) value.

2.8 An Example

In order to illustrate the use of the waiting-time model, consider a satellite system with a terminal in Crawford Hill, NJ at an uplink frequency of 30 GHz[*]. By combining the nominal value of $P_{RAIN} = 0.056$ (from Section 2.3)

---

[*]A 44-GHz example might be prepared by using the frequency dependence illustrated by the NJ and ENG data and extrapolating 30-GHz data to 44 GHz.
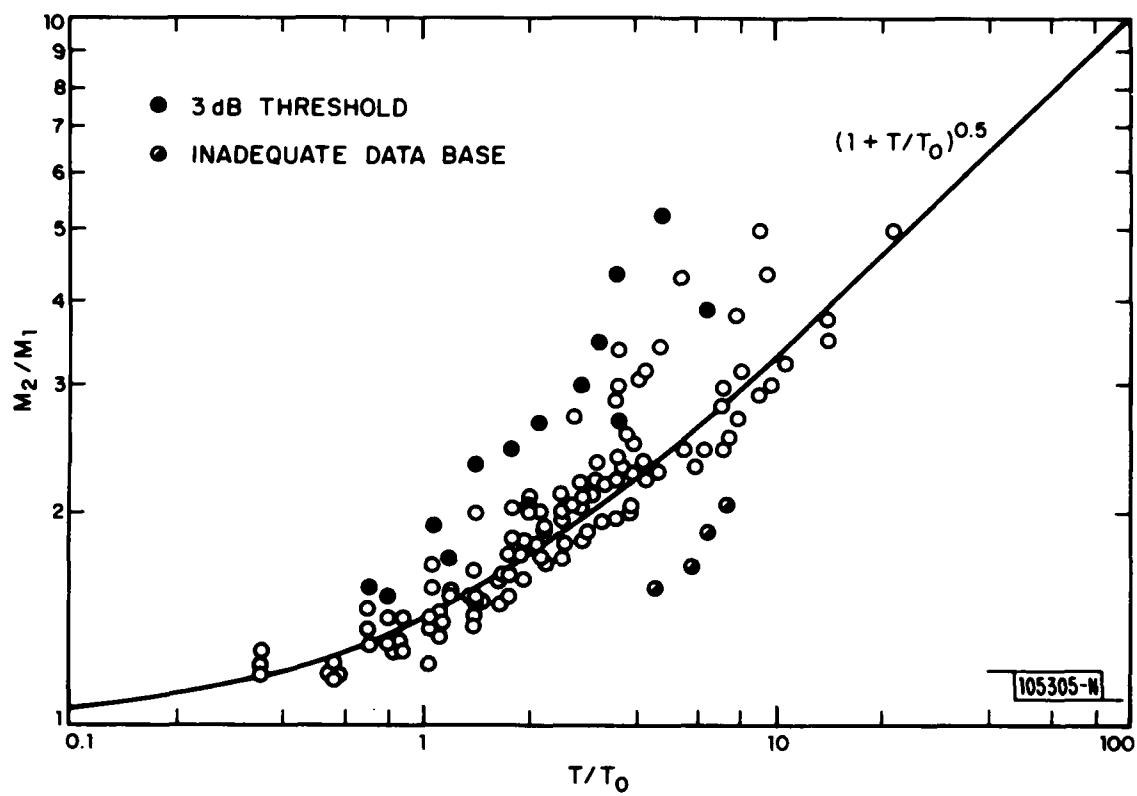
60

Fig. 2.7.2. Composite data for all sites normalized to give M_2/M_1 versus T/T_o.

for the location with the lognormal distribution for the attenuation (from Section 2.6), a yearly availability curve can be generated. Note that the resulting availability function as given in Fig. 2.8.1 is not lognormal[*].

For the nominal values of $D_T=24$ and $D_R=106$, from Section 2.3, the storage-time relationship from (2.7.3) becomes

$$M_2/M_1 = [1 + 0.462T]^{0.5} \qquad (2.8.1)$$

for T-minutes of storage. The resulting improvement in availability with T=1,3,10,30 and 100 minutes is illustrated on Fig. 2.8.1. The curves are not continued much below 3 dB because it is expected that the model becomes progressively more inaccurate as the initial margin becomes less than 3 dB.

Note that slightly less than 20 minutes of storage will produce an order-of-magnitude increase in availability over a wide range of initial margins. At 25 dB of margin, for example, the availability is increased from 0.999 to 0.9999 by supplying the system with 20-minute data-storage capability. The same increase in availability without storage would require increasing the margin from 25 to about 80 dB. At lower initial margins somewhat more storage is required to produce the order-of-magnitude increase (e.g., at 6 dB for M_1 over 30 minutes of storage is necessary).

Although it would seem that an availability producing an average outage of 1 hour per year (~0.9999) would reach an availability of 1.0 with 1 hour of storage, such is not so. The 1 hour figure is for an average year and there is still a quite finite probability that the outage could be well in excess of 1 hour if it was only likely to occur once every several years. Therefore, the 100-minute curve in Fig. 2.8.1 does not produce a unity availability.

---

[*]Obviously, the availability must be greater than $1-P_{RAIN}$ regardless of how hard (or long) it may rain.
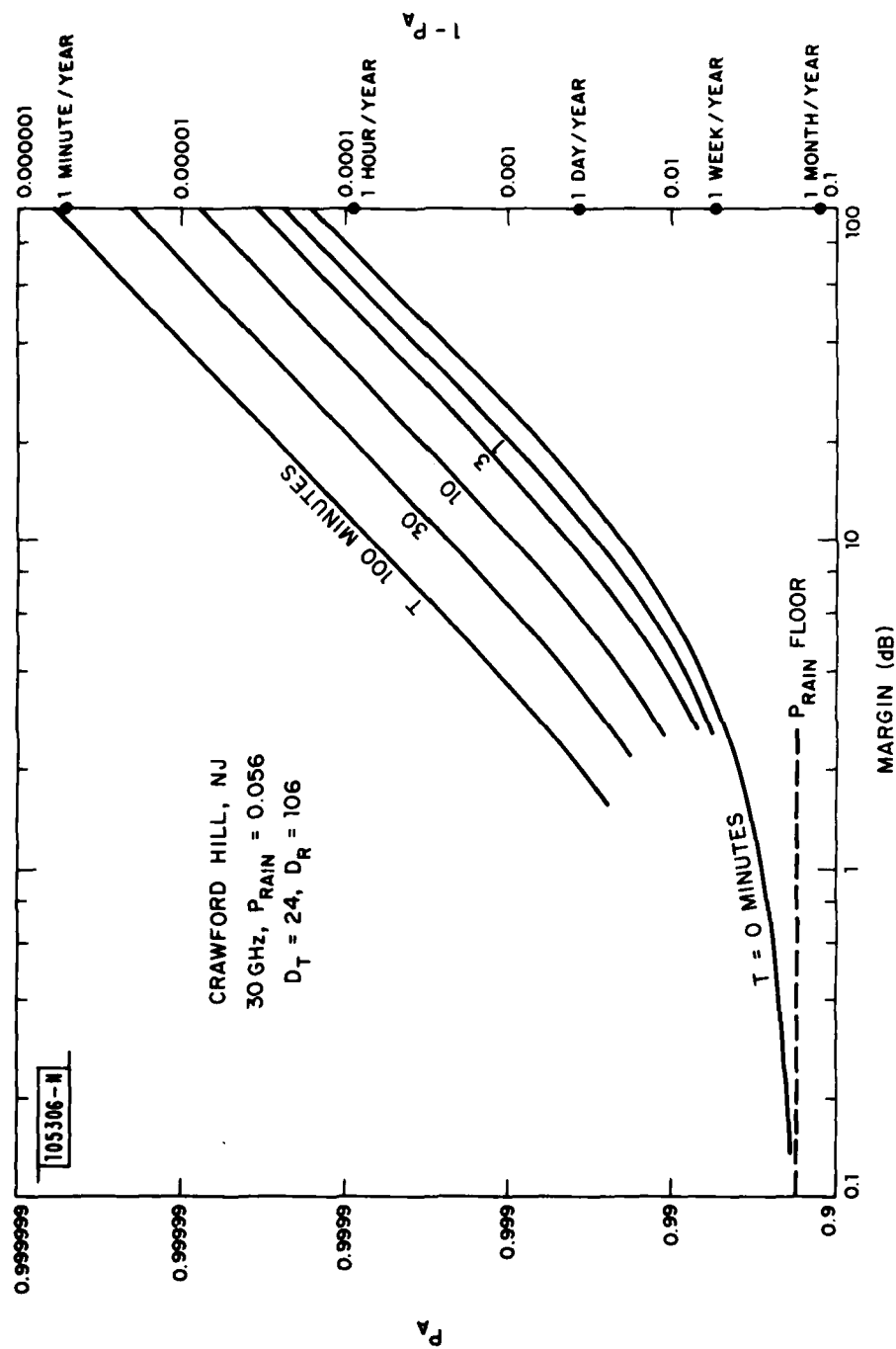
62

Fig. 2.8.1. Availability versus margin and storage time for Crawford Hill, N.J. at 30 GHz.

63

III.   CONCLUDING REMARKS – FUTURE WORK

Utilizing the rather limited attenuation data available, a model for the effect of storage time on rain-induced EHF availability can be developed. The model appears to be "universal" and seems applicable to virtually any climatologic region. The parameters which generate the model are readily available from the standard climatological data for any location on the globe where such data is regularly gathered.

The improvement in effective margin can be written as

$$M_2/M_1 = 1 + 0.2 \; T \; e^{3.7 \; D_T/D_R} \quad 0.5 \tag{3.1}$$

where

T is the data storage time in minutes,

D_T is the number of thunderstorm days/year,

D_R is the number of days/year of rain (defined as the number of days/year of precipitation over 0.25 mm minus the number of days/year of snowfall greater than 25.4 mm)

M_1 is the link margin in dB with no storage, and

M_2 is the equivalent link margin in dB with storage of T minutes available

It seems reasonable to expect that additional data would result in some change in the parameter characterizing (3.1), but the general behavior should remain unchanged.

The determination of long-term attenuation distributions and fade-duration distributions is a difficult and time-consuming task. Much of the data gathering and manipulation could, however, be automated and accumulated virtually in real time, if appropriate hardware were developed and distributed to many of the satellite ground stations. More EHF beacons should be packaged onto available platforms. If such a program were implemented, it would be necessary to choose an ensemble of sites which provide a good sample of the various climatologic regions, in particular those regions with a very low incidence of thunderstorm activity.

BIBLIOGRAPHY

Atlas, D., "Some Experimental Results of Quantitative Radar Analysis of Rainstorms," Memo AWNW 7-4, Part II, All Weather Flying Division, Air Material Command (1948).

Bodtmann, W. F. and C. L. Ruthroff, "Rain Attenuation on Short Radio Paths: Theory, Experiment and Design," Bell Syst. Tech. J. 53, 1329 (1974).

Bussey, H. E., "Microwave Attenuation Estimated from Rainfall and Water Vapor Statistics," Proc. IRE 38, 781 (1950).

Crane, R. K., "Propagation Phenomena Affecting Satellite Communications Systems Operating in the Centimeter and Millimeter Wavelength Bands," Proc. IEEE 59, 173 (1971).

Crane, R. K., P. J. Feteris, K. R. Hardy, C. A. Grainger, and S. H. Cohen, "The 1977 Field Program in Colby-Goodland, Kansas," ERT Document P-1552-IP-3, Environmental Research and Technology, Inc., Concord, MA (1977).

Crane, R. K. and D. W. Blood, "Handbook for the Estimation of Microwave Propagation Effects - Link Calculations for Earth-Space Paths," ERT Document P-7376-TR1, Environmental Reseach and Technology, Inc., Concord, MA (1979).

Crane, R. K., "Attenuation Event Duration Model," ERT Document P-A425, Environmental Research and Technology, Inc., Concord, MA (1980).

Davis, P. G., "Radiometer Studies of Atmospheric Attenuation of Solar Emission at 19 GHz," Proc. IEE 118, 737 (1971).

Davis, P. G., "Slant Path Attenuation at Frequencies Above 10 GHz," IEE Conf Pub. No. 98, 141-149, 10-13 April 1973.

Engelbrecht, R. S., "The Effect of Rain on Satellite Communications Above 10 GHz," RCA Rev. 40, 191 (1979).

Fletcher, R. D., "A Relation Between Maximum Observed Point and Area Rainfall Values," Trans. Amer. Geophys. Union 31, 344 (1950).

Freeny, A. E. and J. D. Gabbe, "A Statistical Description of Intense Rainfall," Bell Syst. Tech. J. 48, 1789 (1969).

Goldhirsh, J., "Path Attenuation Statistics Influenced by Orientation of Rain Cells," IEEE Trans. Antennas Propag. AP-24, 792 (1976).

Handbook of Geophysics, USAF Air Research and Development Command, Geophysics Research Directorate (MacMillan, New York, 1961).

Hogg, D. C., "Statistics on Attenuation of Microwaves by Intense Rain," Bell Syst. Tech. J. 48, 2949 (1969).

Hogg, D. C. and T. S. Chu, "The Role of Rain in Satellite Communications," Proc. IEEE 63, 1308 (1975).

Ippolito, L. J., "Millimeter Wave Propagation and Communications Experiments at 20 and 30 GHz," IEEE Trans. Aerospace Electron. Systems AES-11, 1167 (1975).

Ippolito, L. J., Millimeter Wave Space Communications, Notes for Course No. 501, Continuing Engineering Education Program, George Washington University, Washington, D. C. (22-24 February 1978).

Kaul, R., R. Wallace and G. Kinal, "A Propagation Effects Handbook for Satellite Systems Design," ORI TR-1679, NASA Communications Division, Washington, D. C. (March 1980).

Lin, S. H., "Statistical Behavior of Rain Attenuation," Bell Syst. Tech. J. 52, 557 (1973).

Lin, S. H., "A Method for Calculating Rain Attenuation Distributions on Microwave Paths," Bell Syst. Tech. J. 54, 1051 (1975).

Lin, S. H., "Dependence of Rain-Rate Distribution on Rain-Gauge Integration Time," Bell Syst. Tech. J. 55, 135 (1976a).

Lin, S. H., "Rain-Rate Distributions and Extreme-Value Statistics," Bell Syst. Tech. J. 55, 1111 (1976b).

Local Climatological Data: National Summary, various years, US Department of Commerce, National Oceanic and Atmospheric Administration, National Climatic Center, Federal Building, Asheville, NC, 28801. Also available from Superintendent of Documents, Government Printing Office, Washington, DC 20402.

Monthly Climatic Data for the World, various years, US Department of Commerce, National Oceanic and Atmospheric Administration, National Climatic Center, Federal Building, Asheville, NC, 28801. Also available from Superintendent of Documents, Goverment Printing Office, Washington, DC 20402.

Nackoney, O. G., "CTS 11.7 GHz Propagation Measurements: Second Year's Data Report," Technical Report TR 79-471.2, GTE Laboratories, Waltham, MA (September 1979).

Rogers, R. R., "Statistical Rainstorm Models: Their Theoretical and Physical Foundations," IEEE Trans. Antennas Propag. AP-24, 547 (1976).

Ruffner, J. A., Climates of the States, 1,2, (Gale Research Company, Detriot, MI, 1978).

Strickland, J. I., "Radar Measurements of Site-Diversity Improvement During Precipitation," J. Rech. Atmos. 8, 451 (1974).

Tang, D. D.,"19/29 GHz Propagation Experiment - 1978 Annual Report," Technical Report TR 79-471.4, GTE Laboratories, Waltham, MA (November 1979).

Tang, D. D., GTE Laboratories, Waltham, MA, personal communication (July 1980).

Vogel, W. J., "CTS Attenuation and Cross Polarization Measurements at 11.7 GHz," Final Report: 1 February 1978 to 31 January 1979, Electrical Engineering Research Laboaratory, University of Texas, Austin, TX (1979).

Wilson, R. W., "Sun Tracker Measurements of Attenuation by Rain at 16 and 30 GHz," Bell Syst. Tech. J. 48, 1383 (1969).

Worldwide Airfield Climatic Data, Volume X Part 2 Europe (Low Countries and British Isles), (USAF Environmental Technical Applications Center, Washington, DC, 1971).

ACKNOWLEDGMENT

REPORT DOCUMENTATION PAGE		READ INSTRUCTIONS BEFORE COMPLETING FORM
1. REPORT NUMBER ESD-TR-80-236	2. GOVT ACCESSION NO.	3. RECIPIENT'S CATALOG NUMBER
4. TITLE (and Subtitle) Rain-Outage Reduction by Data Storage in EHF SATCOM Systems		5. TYPE OF REPORT & PERIOD COVERED Project Report
		6. PERFORMING ORG. REPORT NUMBER Project Report DCA-10
7. AUTHOR(s) Robert P. Rafuse		8. CONTRACT OR GRANT NUMBER(s) F19628-80-C-0002
9. PERFORMING ORGANIZATION NAME AND ADDRESS Lincoln Laboratory, M.I.T. P.O. Box 73 Lexington, MA 02173		10. PROGRAM ELEMENT, PROJECT, TASK AREA & WORK UNIT NUMBERS Program Element No. 33126K
11. CONTROLLING OFFICE NAME AND ADDRESS Defense Communications Agency 8th Street and So. Courthouse Road Arlington, VA 22204		12. REPORT DATE 25 November 1980
		13. NUMBER OF PAGES 80
14. MONITORING AGENCY NAME & ADDRESS (if different from Controlling Office) Electronic Systems Division Hanscom AFB Bedford, MA 01731		15. SECURITY CLASS. (of this report) Unclassified
		15a. DECLASSIFICATION DOWNGRADING SCHEDULE

16. DISTRIBUTION STATEMENT (of this Report)

Approved for public release; distribution unlimited.

17. DISTRIBUTION STATEMENT (of the abstract entered in Block 20, if different from Report)

18. SUPPLEMENTARY NOTES

19. KEY WORDS (Continue on reverse side if necessary and identify by block number)

EHF rain attenuation   communications availability satellite

20. ABSTRACT (Continue on reverse side if necessary and identify by block number)

A relationship with apparent geographical universality is developed which allows the calculation of the effective increase in EHF SATCOM rain-induced availability achieved by storing incoming data for later retransmission at a higher rate.